

Light absorption by suspended particles in the Red Sea: effect of phytoplankton community size structure and pigment composition

Malika Kheireddine¹, Mustapha Ouhssain^{1,2,3}, Emanuele Organelli⁴, Annick Bricaud^{2,3}, and Burton H. Jones¹

¹King Abdullah University of Science and Technology (KAUST), Red Sea Research Center (RSRC), Biological and Environmental Sciences and Engineering Division (BESE), Thuwal, 23955-6900, Saudi Arabia

²Sorbonne Universités, UPMC Univ Paris 06, UMR 7093, LOV, Observatoire Océanologique, F-06230 Villefranche-Sur-Mer, France

³CNRS, UMR 7093, LOV, Observatoire Océanologique, F-06230 Villefranche-Sur-Mer, France

⁴Plymouth Marine Laboratory, Plymouth

*** Correspondence:**

Malika Kheireddine

malika.kheireddine@kaust.edu.sa

Abstract

The light absorption properties of phytoplankton ($a_{ph}(\lambda)$) and non-algal particles ($a_{nap}(\lambda)$) associated with phytoplankton pigments were analyzed across the Red Sea, in the upper 200 m depth, between October 2014 and August 2016. The contribution by non-algal particles to the total particulate light absorption ($a_{ph}(\lambda) + a_{nap}(\lambda)$) was highly variable ($23 \pm 17\%$ at 440 nm) and no relationship between $a_{nap}(440)$ and chlorophyll *a* concentration, [TChl *a*], was observed. Phytoplankton specific phytoplankton absorption coefficients at 440 and 676 nm for a given [TChl *a*], $a_{ph}^*(440)$ and $a_{ph}^*(676)$, were slightly higher than those derived from average relationships for open ocean waters within the surface layer as well as along the water column. Variations in the concentration of photosynthetic and photoprotective pigments were noticeable by changes in phytoplankton community size structure as well as in $a_{ph}^*(\lambda)$. This study revealed that a higher proportion of picophytoplankton and an increase in photoprotective pigments (mainly driven by zeaxanthin) tended to be responsible for the higher $a_{ph}^*(\lambda)$ values found in the Red Sea as compared to other oligotrophic regions with similar [TChl *a*]. Understanding this variability across the Red Sea may help improve the accuracy of biogeochemical parameters, such as [TChl *a*], derived from *in situ* measurements and ocean color remote sensing at a regional scale.

1 **1. Introduction**

2 Light absorption coefficients by suspended particles, $a_p(\lambda)$, i.e., phytoplankton ($a_{ph}(\lambda)$) plus
3 non-algal particles ($a_{nap}(\lambda)$), are key parameters that determine the optical signature of
4 oceanic waters and affect the colour of the ocean. The natural variability of these coefficients
5 in various oceanic regions has been studied to establish global bio-optical relationships.
6 Based on these studies, algorithms for the retrieval of biogeochemical products (e.g., [TChl
7 a]) from in situ or ocean colour remote sensing have been refined (Atlas & Bannister, 1980,
8 Morel & Bricaud, 1981; Kiefer & Mitchell, 1983; Morel, 1991; Roesler & Perry, 1995;
9 Garver & Siegel, 1997; Morel & Maritorena, 2001; Sathyendranath et al., 2001; Maritorena
10 et al., 2002; Morel et al., 2006). Furthermore, these coefficients, and the phytoplankton
11 specific phytoplankton absorption coefficient ($a_{ph}^*(\lambda)$) in particular, are also relevant for
12 primary production models and for inferring phytoplankton size and taxonomic composition
13 (Platt & Sathyendranath, 1988; Sathyendranath & Platt, 1988; Ciotti & Bricaud, 2006; Uitz et
14 al., 2010; Tilstone et al., 2014; Bracher et al., 2017). Indeed $a_{ph}^*(\lambda)$ is, at the first order,
15 driven by the concentration in phytoplankton biomass (Mitchell & Kiefer, 1988; Cleveland,
16 1995; Bricaud et al., 1998, 2010) and, at the second order, by phytoplankton size and
17 taxonomic structure as well as pigment composition and proportions (Bricaud et al., 1995,
18 2004; Ciotti et al., 2002; Ciotti & Bricaud, 2006; Devred et al., 2006). Thus, understanding
19 the variability of $a_{ph}^*(\lambda)$ with respect to [TChl a], phytoplankton community structure and
20 pigment composition is of primary relevance for biogeochemical studies and ocean colour
21 remote sensing applications (Morel & Bricaud, 1981; Roesler & Perry, 1995; Sathyendranath
22 et al., 2001).

23 While the variations in $a_{ph}(\lambda)$ and $a_{nap}(\lambda)$ have been extensively studied in various area of the
24 global ocean (Bricaud et al., 1995, 1998, 2010; Lutz et al., 1996; Suzuki et al., 1998; Devred

25 et al., 2006; Boss et al., 2013), few studies have been performed in the Red Sea (Brewin et
26 al., 2015, Organelli et al., 2017) during the last three decades. Recently, Brewin et al. (2015)
27 suggested that the Red Sea waters and their optical characteristics can be affected by its
28 different hydrological, biological and environmental conditions (low precipitation, little
29 riverine input, and desert dust events), giving rise to distinct bio-optical relationships in some
30 subareas of this sea. Using field or ocean colour remote sensing observations to infer
31 biogeochemical parameters (e.g., $a_{ph}(\lambda)$, [TChl a]) from previously established bio-optical
32 models, therefore, may introduce uncertainties in the retrieved products (Organelli et al.,
33 2017). When analyzing the bio-optical characteristics of the Red Sea, Brewin et al. (2015)
34 observed that the relationship established between the particulate backscattering coefficient
35 and [TChl a] as well as the relationship between $a_p(\lambda)$ and [TChl a] were similar to those
36 parameterized by Brewin et al. (2012) and Bricaud et al. (1998) for other clear waters,
37 respectively. Thus, they suggested that the overestimation of remotely-sensed [TChl a]
38 concentrations in the Red Sea, as derived from standard bio-optical algorithms, could be due
39 to an excess of colored dissolved organic matter (CDOM) absorption per unit of [TChl a].
40 However, Organelli et al. (2017) did not observe bio-optical anomalies in the Red Sea, when
41 analyzing measurements of diffuse attenuation coefficient for downward irradiance at those
42 wavelengths used as proxies of CDOM and phytoplankton light absorption coefficients
43 (Morel et al., 2007). In these studies, measurements were only taken during a limited period
44 of the year (fall-winter season), either restricted to the surface layer or in a given sub-region
45 of the Red Sea. It is now well known that changes in optical properties can depend on
46 modifications of proportions between the optically significant substances (CDOM, non-algal
47 particles and phytoplankton) observed over seasons (Sathyendranath et al., 1999; Devred et
48 al., 2006; Organelli et al., 2014). Therefore, further characterization of the bio-optical
49 behavior of the Red Sea is required.

50 The Red Sea is one of the most saline and warmest deep seas in the world (Belkin, 2009;
51 Longhurst, 2007; Raitzos et al., 2011, 2013) characterized by low precipitation, little riverine
52 input (Patzert, 1974) and high evaporation rates (Sofianos & Johns, 2003). The Red Sea
53 displays pronounced south-north latitudinal gradients in environmental conditions such as
54 temperature, salinity, light intensity and nutrients (Neumann & McGill, 1962; Sofianos &
55 Johns, 2002; Raitzos et al., 2013; Churchill et al., 2014; Sawall et al., 2014; Ismael, 2015).
56 The Red Sea is considered as a large marine ecosystem (Belkin, 2009) and sustains coral
57 reefs, mangroves and seagrass beds, which provide habitat for a large variety of marine
58 organisms (Berumen et al., 2013; Almahasheer et al., 2016). The Red Sea is known as an
59 oligotrophic basin given the depletion of nutrients in the surface layer (Raitzos et al., 2013,
60 2015; Triantafyllou et al., 2014; Racault et al., 2015).

61 Several studies showed that the seasonal variability of phytoplankton biomass in the Red Sea
62 appears to be controlled by physical processes (winter mixing, mesoscale eddies, horizontal
63 advection and intrusion of water masses from Bab-el-Mandeb) that determine the availability
64 of nutrients to the euphotic layer (Raitzos et al., 2013, 2015; Triantafyllou et al., 2014;
65 Racault et al., 2015; Dreano et al. 2016; Wafar et al. 2016; Gittings et al. 2017). Recently,
66 Pearman et al. (2016) and Kheireddine et al. (2017) showed that phytoplankton community
67 structure (size and taxonomy) and its spatio-vertical distribution appear to adapt in response
68 to changes in environmental conditions along the south-north latitudinal gradients. They
69 observed that picophytoplankton were generally the most abundant group at the surface along
70 the whole basin. Nanophytoplankton, such as pelagophytes and prymnesiophytes, mainly
71 characterized the community structure below the surface down to a depth of 150 m. In the
72 southern Red Sea, microphytoplankton (diatoms) were more prominent at the bottom of the
73 euphotic layer. Pearman et al. (2016) suggested that this distribution correlated with increased
74 nutrients found in this region, caused by the inflow of nutrient-rich water from the Gulf of

75 Aden. How this variability in phytoplankton size structure, and thus in photosynthetic and
76 photoprotective pigment concentrations, influences both $a_{ph}(\lambda)$ and $a^*_{ph}(\lambda)$ along the water
77 column remains unknown.

78 A unique dataset of High-Performance Liquid Chromatography-derived phytoplankton
79 pigments and spectral light absorption coefficients of phytoplankton and non-algal particles
80 has been compiled for the upper 200 m water column across the Red Sea basin. This dataset
81 will increase the understanding of the bio-optical properties of this region and, with a focus
82 on surface waters, evaluate the feasibility to retrieve biogeochemical quantities with better
83 accuracy from ocean colour observations. In particular, this study aims to (1) examine the
84 relationships linking $a_p(\lambda)$, $a_{ph}(\lambda)$ and $a_{nap}(\lambda)$ to phytoplankton biomass ([TChl a]), (2) assess
85 the influences of phytoplankton cell size and pigment composition on the variability in light
86 absorption properties and (3) identify presence/lack of consistency between the bio-optical
87 relationships established in Red Sea waters and those parameterized for other oceanic areas
88 around the world.

89

90 **2. Materials and methods**

91 *2.1 Oceanographic cruises and sampling---* Samples were collected during five research
92 cruises performed across the Red Sea between October 2014 and January 2016 on board of
93 the R/V Thuwal. Two cruises named as CRS-01, and CRS-04 took place in the central Red
94 Sea (CRS) during fall and winter, specifically from 16 - 28 October 2014 and from 17 - 28
95 January 2016, respectively. Two cruises, Duba-01 and Duba-02 were conducted in the
96 northern Red Sea (NRS) in spring during the periods of 17 - 28 April 2015 and 21 March - 2
97 April 2016, respectively. A cruise to Jazan took place in the southern Red Sea (SRS) in
98 winter from 8 - 21 February 2015. A total of 40 stations were sampled: 18 in the NRS, 14 in
99 the CRS and 8 in the SRS (Fig. 1) (Table 1).

100 Discrete seawater samples for determining phytoplankton pigment concentrations and
101 particulate absorption spectra were collected using a rosette system equipped with 10 L
102 Niskin bottles at typically 10 depths within the upper 200 m depth of the water column (5, 10,
103 20, 40, 50, 60, 70, 80, 150 and 200 m). Temperature and salinity profiles were obtained using
104 a SBE 9 (Sea-Bird Electronics) Conductivity-Temperature-Depth (CTD) probe. The dataset
105 consisted of 297 measurements of absorption spectra and phytoplankton pigment
106 concentrations. The first optical depth, that corresponds to the surface layer observed by
107 satellite ocean color sensors (Gordon & McCluney, 1975), was obtained as the euphotic
108 depth, Z_e , divided by 4.6 (Morel, 1988). Z_e is the depth at which PAR decreases to 1% of its
109 value ($\ln(1\%) = -4.6$) just below the sea surface, and was derived from [TChl *a*]
110 concentration profiles (Morel & Maritorena, 2001).

111 *2.2 Phytoplankton pigment analysis*--- Seawater samples (with volume ranging from 2.3 L to
112 2.8 L) were filtered through 25 mm diameter Whatman GF/F filters (0.7 μm porosity), stored
113 in liquid nitrogen during the cruise and subsequently at -80 °C in the laboratory until
114 analysis. A total of 25 pigments were quantified using a High Performance Liquid
115 Chromatography (HPLC) complete 1260 Agilent Technologies system according to the
116 protocol described in Ras et al. (2008). Briefly, filters were ground in 3 ml of 100% methanol
117 together with glass beads of 1 mm diameter by cell homogenizer. The extract was centrifuged
118 for ten minutes at 7500 rpm and cooled at -5 °C. Then the supernatants were filtered through
119 a Teflon syringe filter of 0.2 μm and the extracts were analyzed.

120 In this study, the sum of concentrations of chlorophyll *a*, divinyl chlorophyll *a*,
121 chlorophyllide *a*, and phaeo was used as an index of phytoplankton biomass and noted [TChl
122 *a* + phaeo]. The term phaeo includes the sum of phaeophytin *a* and phaeophorbide *a*
123 pigments. The total chlorophyll b concentration, noted [TChl b], and the total chlorophyll c
124 concentration, noted [TChl c], were computed as the sum of the concentrations of chlorophyll

125 b and divinyl chlorophyll b and chlorophyll c1, c2 and c3, respectively. Photosynthetic
126 carotenoids (PSC) correspond to the sum of fucoxanthin (Fuco), peridinin (Peri), 19'
127 hexanoyloxyfucoxanthin (19'HF) and 19'-butanoyloxyfucoxanthin (19'BF), while
128 nonphotosynthetic carotenoids (PPC) include zeaxanthin (Zea), alloxanthin (Allo),
129 diadinoxanthin (Diadi), diatoxanthin (Diato), β -carotene, lutein (Lut), violaxanthin (Viola),
130 and neoxanthin (Neo).

131 *2.2.1 Estimation of phytoplankton size based on pigments---* Diagnostic accessory pigments
132 considered as biomarkers of specific phytoplankton taxonomic groups and size classes
133 (Vidussi et al., 2001) were used to determine the relative proportions of pico- (< 2 μ m), nano-
134 (2-20 μ m) and microphytoplankton (> 20 μ m). The biomass proportions associated with each
135 size class were computed from pigment ratios following Uitz et al. (2006):

$$136 \quad \% \text{ micro} = 100 * (1.41 [\text{Fuco}] + 1.41 [\text{Peri}]) / \text{DP} \quad (1)$$

$$137 \quad \% \text{ nano} = 100 * (0.6 [\text{Allo}] + 1.27 [19'\text{HF-Fuco}] + 0.35 [19'\text{BF-Fuco}]) / \text{DP} \quad (2)$$

$$138 \quad \% \text{ pico} = 100 * (0.86 [\text{Zea}] + 1.01 [\text{TChl b}]) / \text{DP} \quad (3)$$

139 where DP is the sum of the seven diagnostic pigment concentrations:

$$140 \quad \text{DP} = 1.41 [\text{Fuco}] + 1.41 [\text{Peri}] + 0.6 [\text{Allo}] + 0.35 [19'\text{BF-Fuco}] + 1.27[19'\text{HF-Fuco}] \quad (4)$$

$$141 \quad + 0.86 [\text{Zea}] + 1.01 [\text{TChlb}]$$

142 This approach has notable limitations. Some diagnostic pigments are shared by several
143 phytoplankton groups and some groups may cover a broad size range, such as zeaxanthin
144 containing *Trichodesmium* (microphytoplankton), or 19'BF and 19'HF in some picoplankton
145 prymnesiophytes. This approach is not compared with others techniques such as flow
146 cytometry, microscopy and molecular analysis. However, several previous studies
147 demonstrated good performances of this method in providing the dominant trends of the

148 phytoplankton community size structure in other oligotrophic regions of the world's oceans
149 (Uitz et al., 2008, 2015; Ras et al., 2008; Organelli et al., 2013).

150 The size index (SI) was derived from the proportions of pico-, nano- and microphytoplankton
151 to provide a single indicator of the dominant phytoplankton community size structure
152 (Bricaud et al., 2004). SI was computed as follows:

$$153 \quad \text{SI} = (1*[\% \text{pico}] + 5*[\% \text{nano}] + 50*[\% \text{micro}]) / 100 \quad (5)$$

154 where 1 μm , 5 μm and 50 μm are taken as central size values for each phytoplankton class
155 (Bricaud et al., 2004).

156 *2.3 Particulate absorption measurements---* Particulate absorption spectra, $a_p(\lambda)$, were
157 measured using a quantitative filter pad technique (Mitchell et al., 2003). Seawater samples
158 (2.3 L to 2.8 L) were filtered on Whatman GF/F filters (0.7 μm porosity) and stored in liquid
159 nitrogen during the cruise and subsequently at -80 °C in the laboratory until analysis.
160 Particulate absorption spectra were measured, with a Varian Cary 5000 double-beam
161 Ultraviolet-Visible-Infrared spectrophotometer equipped with an integrating sphere, in the
162 300-800 nm spectral range at 1 nm intervals. A blank wet filter (pure water) was used as a
163 reference. We used this equipment with samples placed inside the integrating sphere, which
164 allowed us to minimize the scattering error and to determine whether significant absorption
165 exists in the near infrared. All spectra were converted into $a_p(\lambda)$ (in m^{-1}) and then corrected
166 for the path-length amplification effect according to Stramski et al. (2015).

167 The respective contributions of phytoplankton ($a_{ph}(\lambda)$) and non-algal particles ($a_{nap}(\lambda)$) to total
168 particulate absorption were determined by numerical decomposition (Bricaud & Stramski,
169 1990).

170 A few samples ($N=21$) were also analyzed using the method of Kishino et al. (1985), based
171 on the pigment extraction in methanol. Absorption ratios derived from these $a_{ph}(\lambda)$ spectra

172 were found to be very close to the standard ratios used in the numerical decomposition. In
173 addition, the comparison between $a_{ph}(\lambda)$ and $a_{nap}(\lambda)$ spectra obtained using the method of
174 Kishino et al. (1985) and those estimated from numerical decomposition was high ($R^2=0.96$,
175 slope=1.03; $R^2=0.88$, slope=1.08; $N=21$, $p<0.0001$, respectively) confirming the validity of
176 the method established by Bricaud and Stramski, (1990) for Red Sea waters.

177 Phytoplankton specific values of phytoplankton absorption coefficients, $a_{ph}^*(\lambda)$, were
178 computed by dividing $a_{ph}(\lambda)$ by [TChl a].

179 *2.4 Estimation of phytoplankton size based on the phytoplankton absorption spectrum---* An
180 estimation of the phytoplankton size factor, S_f , was computed based on the shape of the
181 phytoplankton absorption spectrum as described by Ciotti et al. (2002). The model developed
182 by Ciotti et al. (2002) reconstructs the shape of any phytoplankton absorption spectrum
183 (normalized by the mean in the 400-700 nm range) using a linear combination of two spectra
184 corresponding to pure picophytoplankton and microphytoplankton populations. Note that the
185 picophytoplankton vector used here was provided by Ciotti and Bricaud, (2006). The values
186 of S_f vary from 0 to 1. S_f tends to 0 for a population composed exclusively of
187 microphytoplankton and to 1 for a pure picophytoplankton assemblage. Values of S_f
188 comprised between 0 and 1 represent all possible conditions between these two extremes. The
189 accuracy of the spectral fit was assessed for each phytoplankton absorption spectrum by
190 computing the coefficient of correlation, R^2 , between all spectral values and those
191 reconstructed by the model. Values of S_f corresponding to $R^2 \geq 0.97$ (RMSE = $0.073 \pm$
192 0.022) between measured and reconstructed phytoplankton absorption spectra were retained
193 (92% of the entire database).

194 **3. Results and Discussion**

195 *3.1 Particulate, phytoplankton and non-algal particles absorption coefficients as a function*
196 *of [TChl a]---* Variations of $a_p(\lambda)$, $a_{ph}(\lambda)$ and $a_{nap}(\lambda)$ as a function of [TChl a] are displayed in
197 Figures 2 and 3 and are compared with the global relationships established for oligotrophic
198 waters using in situ measurements in various regions of the global ocean. With reference to
199 ocean colour remote sensing, the analyses of $a_p(\lambda)$, $a_{ph}(\lambda)$ and $a_{nap}(\lambda)$ as a function of [TChl a]
200 was also restricted to the first optical depth. The regression formula in the form of a power
201 law for each relationships between the parameter of interest and [TChl a] are presented in
202 Table 2.

203

204 *3.1.1 Particulate absorption coefficients as a function of [TChl a]---*The a_p values at 440 and
205 676 nm within the surface layer are significantly correlated to [TChl a] ($R^2=0.87$ and 0.89 ,
206 respectively, $N=108$, $p<0.0001$) as well as when considering all samples from the upper 200
207 m depth ($R^2=0.85$ and 0.88 , respectively, $N=297$, $p<0.0001$) (Fig. 2A, B). The $a_p(\lambda)$ versus
208 [TChl a] relationships obtained using measurements limited to the first optical depth
209 significantly differ from those established when all depths were considered ($p < 0.05$ for all,
210 ANCOVA test). We also found that our measurements, which were collected both within the
211 surface layer and in all depths, were slightly higher for a given [TChl a] than those of Bricaud
212 et al. (1998), for the global ocean, and Brewin et al. (2015), for the Red Sea, over the whole
213 range of our measurements ([TChl a] = 0.006 to 1 mg.m^{-3}) (Fig. 2A, B).

214 The relationships obtained using measurements limited to the surface layer differ statistically
215 with those established when all depths were considered ($p < 0.05$ for all, ANCOVA test). We
216 found that our measurements, which have been collected both within the surface layer and in
217 all depths, were slightly above those of Bricaud et al. (1998), for the global ocean, and
218 Brewin et al. (2015), for the Red Sea, over the whole range of our measurements ([TChl
219 a]= 0.006 to 1 mg.m^{-3}) (Fig. 2A, B).

220 Possible reasons for the differences between our results and those of Brewin et al. (2015) may
221 be attributed to the use of HPLC-measured [TChl *a*] in this study. Brewin et al. (2015)
222 obtained [TChl *a*] from a_p measurements at 650, 676 and 715 nm (Line Height method) in
223 Red Sea waters. Although this method has been found to perform well in various areas of the
224 global ocean (Boss et al., 2007, 2013b; Dall'Olmo et al., 2009, 2012; Westberry et al., 2010;
225 Roesler & Barnard, 2013), our results show that a linear fit to our data of [TChl *a*] measured
226 by HPLC versus [TChl *a*] retrieved from $a_p(\lambda)$ provided the equation $[TChl\ a]_{LH} = 1.17 * [TChl\ a]_{HPLC} + 0.0026$ ($R^2 = 0.91$, $N=297$, $p<0.0001$) was not apparent, indicating significant
227 overestimation of [TChl *a*]_{LH} as compared with [TChl *a*]_{HPLC}. Furthermore, Brewin et al.
228 (2015) used a larger number of measurements of $a_p(\lambda)$ below $0.1\ mg\cdot m^{-3}$ compared to our
229 dataset, which could also affect the conclusions in our study.

231 *3.1.2 Phytoplankton absorption coefficients as a function of [TChl *a*]*---The relationships
232 between a_{ph} and [TChl *a*] at 440 and 676 nm are shown in Figure 2C, D. A significantly high
233 correlation is also found between $a_{ph}(\lambda)$ and [TChl *a*] within the surface layer and among
234 depths at 440 nm ($R^2 = 0.89$ and 0.91 , $N=108$ and 297 , respectively, $p<0.0001$) and at 676
235 nm ($R^2 = 0.91$ and 0.92 , $N=108$ and 297 , respectively, $p<0.0001$). As for $a_p(\lambda)$, the
236 relationships between $a_{ph}(\lambda)$ and [TChl *a*] established within the surface waters significantly
237 differ from those established considering all samples between 0 and 200 m depth ($p < 0.05$
238 for both, ANCOVA test).

239 The relationships obtained between $a_{ph}(\lambda)$ and [TChl *a*] within the surface as well as along
240 the water column are above the existing global relationships proposed by Bricaud et al.
241 (1995), Devred et al. (2006) and Brewin et al. (2011) (Fig. 2C, D) ($p < 0.05$ for all,
242 ANCOVA test). Given the relationships established by Devred et al. (2006) and Brewin et al.
243 (2011) are based on a two-population model and not on a power law function, this may affect
244 our comparisons in this study. Indeed, these models relate $a_{ph}(\lambda)$ to [TChl *a*], assuming that

245 the assemblages of phytoplankton comprise mixtures of two populations whose proportions
246 vary as the total concentration of cells changes. On the other hand, the relationship obtained
247 at 440 nm considering all depths is in relatively good agreement with the relationship
248 determined by Bricaud et al. (2004) (Fig. 2C) ($p \geq 0.05$, ANCOVA test), although this
249 relationship is only representative of measurements collected in the surface layer. The
250 relationship of Bricaud et al. (2004) is based on a different dataset (measurements collected
251 in various oceanic regions and trophic states) than the one used in Bricaud et al. (1995) and
252 might explain why the relationship of Bricaud et al. (2004) is more closely aligned to the
253 relationship revealed in this study.

254 *3.1.3 Non-algal particles absorption coefficients as a function of [TChl a]*---No clear
255 relationship between a_{nap} at 440 nm and [TChl a] appears among depths (Fig. 3A). This is in
256 agreement with previous studies performed in oligotrophic waters (Cleveland, 1995). The
257 $a_{\text{nap}(440)}$ values are highly scattered around the relationship established by Bricaud et al.
258 (2010) from data collected in the Pacific Ocean (BIOSOPE area), reflecting different trophic
259 regimes. Furthermore, in the deep layer where [TChl a] varies from 0.006 to 0.1 $\text{mg}\cdot\text{m}^{-3}$,
260 $a_{\text{nap}(440)}$ values are higher than those predicted by this relationship (Fig. 3A). The ratio of
261 non-algal absorption coefficient to particulate absorption at 440 nm, $a_{\text{nap}(440)}/a_{\text{p}(440)}$, as a
262 function of [TChl a] is displayed in Figure 3B. Deep Red Sea waters with low [TChl a]
263 concentrations (0.006-0.1 $\text{mg}\cdot\text{m}^{-3}$) are characterized by high values of $a_{\text{nap}(440)}/a_{\text{p}(440)}$,
264 between 0.45 and 1. This result suggests that the $a_{\text{nap}(440)}/a_{\text{p}(440)}$ varies inversely to [TChl
265 a] in clear Red Sea waters. This is consistent with the observations made in other oligotrophic
266 regions, such as in the Pacific Ocean (Bricaud et al., 2010). Bricaud et al. (2010) suggested
267 that the high contribution of the $a_{\text{nap}(440)}/a_{\text{p}(440)}$ ratio could indicate the presence of a large
268 amount (or more colored) of non-algal particles. The Red Sea is also known as a region
269 where significant inputs from dust occur [Prospero et al., 2002; Ginoux et al., 2012; Al Taani

270 et al., 2015; Prakash et al., 2015]. Frequent dust outbreaks and dust storms have been
271 observed in the Red Sea during our research cruises. Satellite observations
272 (http://neo.sci.gsfc.nasa.gov/view.php?datasetId=MODAL2_M_AER_OD) revealed that
273 Saharan dust events occurred in the entire Red Sea during most of the cruises (CRS-04,
274 Duba-01, Duba-02 and Jazan) performed for this study. The presence of these inorganic
275 particles can partly explain the high contribution of the $a_{\text{nap}}(440)/a_{\text{p}}(440)$ ratio in Red Sea
276 deep waters by increasing the sinking velocity of non-algal particles (Ploug et al., 2008).
277 When [TChl *a*] varies from 0.1 to 1 mg.m⁻³, $a_{\text{nap}}(440)/a_{\text{p}}(440)$ is highly variable with values
278 ranging from 0.028 to 0.45. This is consistent with the values observed in the Pacific Ocean,
279 Mediterranean Sea and Atlantic Ocean (Bricaud et al., 2010). This large variability can be
280 explained by varying contributions of non-algal particles (detritus, bacteria, viruses, inorganic
281 particles) along the water column. Several studies also demonstrated that dust inputs have a
282 positive effect on bacterial growth and abundance, diversity and composition of the
283 indigenous bacterial assemblages (Reche et al., 2009; Lekunberri et al., 2010; Morales-
284 Baquero et al., 2013). Dust deposition can thus affect the proportion of bacteria in Red Sea
285 waters and partly explain the high variability observed in the $a_{\text{nap}}(440)/a_{\text{p}}(440)$ ratio.

286 The above comparisons suggest that the high values of $a_{\text{p}}(\lambda)$ observed within the surface Red
287 Sea waters ([TChl *a*] below 0.1 mg.m⁻³) is mainly related to an important contribution of non-
288 algal particles in these waters (Fig. 2A, B).

289

290 3.2 Phytoplankton size structure associated with phytoplankton absorption spectra---

291 Variability in $a_{\text{ph}}(\lambda)$ is observed in this study (Fig. 2C, B). The variability observed around
292 the relationship between $a_{\text{ph}}(\lambda)$ and [TChl *a*] may be due to changes in phytoplankton
293 community structure. It is generally known that variations in phytoplankton size structure and
294 the intracellular concentrations of diverse phytoplankton pigments induce variations in $a_{\text{ph}}(\lambda)$

295 at a given [TChl *a*] (Sathyendranath et al., 1996; Bricaud et al., 2004, 2010; Organelli et al.,
296 2011; Ferreira et al., 2013).

297 The relative contributions of nano- and picophytoplankton to total algal biomass are high in
298 Red Sea waters (Fig. 4). Based on phytoplankton pigments ratio, we found that
299 picophytoplankton dominate the upper layer in the whole basin due to the presence of
300 *Prochlorococcus sp* and *Synechococcus sp*, but it remains highest in the central part of the
301 basin (>60% of the phytoplankton biomass). The nanophytoplankton group, mainly
302 associated with prymnesiophytes and pelagophytes, is relatively abundant (40-60% of the
303 phytoplankton biomass) below 25 m depth to 180 m depth along the whole basin. The
304 microphytoplankton pool, primarily associated with diatoms, is mainly observed in the
305 southern part (45-75% of phytoplankton biomass) of the basin and were present in low
306 concentrations (5-30% of the total phytoplankton biomass) in the other bioregions (not
307 shown). These observations are consistent with the phytoplankton community size structure
308 generally found in oligotrophic areas of the ocean (Bricaud et al., 2004; Ras et al., 2008;
309 Organelli et al., 2011) and in the Red Sea (Pearman et al., 2016; Kheireddine et al., 2017). As
310 this trend has been discussed in details in Kheireddine et al. (2017) where they studied the
311 spatio-vertical distribution of phytoplankton pigments during similar time periods (Jazan and
312 Duba-01 cruises) or season of sampling, the reader is referred to Kheireddine et al. (2017)
313 and references therein for more information regarding the phytoplankton community size
314 structure distributions in the Red Sea.

315 To examine variations in the shape of the phytoplankton absorption spectra of each
316 phytoplankton size class (micro-, nano- and picophytoplankton), spectra are normalized to its
317 mean value computed on the basis of all spectral values between 400 and 700 nm (Ciotti et
318 al., 2002), and then grouped into the three size classes according to dominance (> 50%).

319 Differences between the average spectra for each dominant community size of phytoplankton
320 can be observed (Fig. 5). For the picophytoplankton dominated spectra, the blue-to-red ratio
321 is higher (2.35) than in nanophytoplankton (2.21) or microphytoplankton (2.16) dominated
322 spectra. This result reflects a stronger package effect for microphytoplankton cells. This is in
323 agreement with previous studies showing that variability in the spectral shape of
324 phytoplankton absorption can be mainly attributed to changes in phytoplankton cell size
325 (Sathyendranath et al., 2001; Ciotti et al., 2002; Lohrenz et al., 2003; Devred et al., 2006;
326 Brewin et al., 2011, Wang et al., 2015). Note that the variations around the mean spectra of
327 picophytoplankton-dominated absorption coefficients reflect a larger variability in the
328 contribution of accessory pigments associated with smaller cells in comparison to those
329 dominated by microphytoplankton (Fig. 5).

330 Ciotti et al. (2002) showed that in the surface layer, the variability in the spectral shape of
331 phytoplankton absorption could be mainly explained by variation in cell size of the major
332 phytoplankton group, thus enabling the development of a model to estimate a cell size
333 parameter for phytoplankton (i.e., S_f). In the present study we estimated S_f for each
334 phytoplankton absorption spectrum. The model of Ciotti et al. (2002) provides estimates of
335 the dominant size of the phytoplankton community that can be compared to the relative
336 proportions of pico-and microphytoplankton that are derived from phytoplankton diagnostic
337 pigments (see methods; Vidussi et al., 2001; Bricaud et al., 2004; Uitz et al., 2006). The
338 values of S_f vary from 0.12 to 0.98 (Fig. 6).

339 S_f decreases when the contribution of microphytoplankton tends to increase (Fig. 6A), and
340 increases with the proportion of picophytoplankton (Fig. 6B). S_f values are in good
341 agreement with the relative proportion of picophytoplankton ($R^2 = 0.63$, $N=297$, $p<0.0001$)
342 and microphytoplankton ($R^2 = 0.44$, $N=297$, $p<0.0001$) despite the scattering observed
343 around these relationships due to the photoacclimation of phytoplankton cells in depth. It is

344 well established that the proportion in accessory pigments vary along the water column
345 (Bricaud et al., 1995; Organelli et al., 2011). For example, photoprotective pigments tend to a
346 continuously decrease from the surface to deeper waters (Bricaud et al., 1995; Organelli et
347 al., 2011; Kheireddine et al., 2017). This can significantly impact the shape of the
348 phytoplankton absorption spectrum. As the model of Ciotti et al. (2002) was established for
349 surface waters, its use for samples collected in depth could reveal photoacclimation responses
350 to the vertical light variation. For example, for the same dominant cell size, the S_f values will
351 tend to decrease if the phytoplankton community shows an increase in the concentrations of
352 intracellular pigments caused, for instance, by photoacclimation (Ciotti et al., 1999).

353 The scattering observed around these relationships could also be partly explained by the fact
354 that the phytoplankton community size is inferred by phytoplankton pigments that may be
355 shared by several phytoplankton size class as mentioned previously. Overall, considering the
356 assumptions in each approach, these results suggest that the absorption-based method
357 developed by Ciotti et al. (2002) is consistent with the approach based on phytoplankton
358 pigments.

359

360 *3.3 Specific phytoplankton absorption variability associated with changes in phytoplankton*
361 *cell size and pigment composition---* As reported in previous studies (Bricaud et al., 1995,
362 2004; Sathyendranath et al., 1996; Allali et al., 1997; Organelli et al., 2011; Ferreira et al.,
363 2013), a_{ph}^* values clearly decrease with increasing [TChl *a*] at 440 nm within the surface
364 layer and among depths ($R^2 = 0.61$, $N=108$ and 297, respectively $p<0.0001$), and slightly
365 decrease at 676 nm only when all depth are considered ($R^2 = 0.44$, $N=297$, $p<0.0001$) (Fig.
366 7). A broad range of variation in [TChl *a*] (0.008-1 $mg.m^{-3}$) is associated with a narrower
367 variability in $a_{ph}^*(676)$ values (0.011-0.036 m^{-1}), whereas $a_{ph}^*(440)$ values vary widely
368 (0.029-0.152 m^{-1}). This observation is consistent with anterior studies in other oligotrophic

369 environments (Bouman et al., 2003; Perez et al., 2007; Organelli et al., 2011, Vijayan et al.,
370 2014). The large variability observed in $a_{ph}^*(440)$ and $a_{ph}^*(676)$ for a given [TChl a] can be
371 attributed to changes in phytoplankton community size structure and pigment composition.
372 The estimations of S_f may help in explaining the variability observed around the relationship
373 between $a_{ph}^*(\lambda)$ and [TChl a] (Fig. 7). In general, the highest $a_{ph}^*(\lambda)$ correspond to higher S_f
374 values, (smaller phytoplankton cell size), and the lower $a_{ph}^*(\lambda)$ to the lower S_f values (larger
375 phytoplankton cell size) (Fig. 7). This is in agreement with the literature (Stuart et al., 1998,
376 Sathyendranath et al., 1999; Roy et al., 2011; Lohrenz et al., 2003; Brunelle et al., 2012;
377 Ferreira et al., 2013; Wang et al., 2015) and reflects an increasing pigment packaging effect
378 with increasing [TChl a] and the dominance of larger phytoplankton cell sizes (Bricaud et al.,
379 1995; Morel et al., 2006; Barlow et al., 2008). Nevertheless, some S_f values ($0.2 < S_f < 0.4$)
380 above the surface layer are not consistent with the general assumption of increasing S_f with
381 increasing $a_{ph}^*(\lambda)$ (Fig. 7). These S_f values are observed for a large variation in [TChl a] that
382 does not conform with the general assumption that S_f values decrease with increasing [TChl
383 a] (Ciotti et al., 2002) in response to photoacclimation processes (Fig. 7). Indeed, such
384 inconsistencies can occur because S_f does not depend only on cell size. It reflects changes in
385 pigment composition and package effect in response to changes in phytoplankton cell size
386 associated with variations in intracellular pigment content from surface to deep waters that
387 affect the spectral shape of phytoplankton absorption (Morel and Bricaud, 1981; Ciotti et al.,
388 2002). For example, Ferreira et al. (2013) have shown that, for the same phytoplankton cell
389 size, S_f values tend to decrease if phytoplankton community shows an increase in the
390 concentrations of intracellular pigments due to photoacclimation (Ciotti et al., 1999). Thus,
391 the parameter S_f cannot be used solely to study changes in phytoplankton cell size as
392 variations in intracellular pigment content will also affect this parameter at a given cell size
393 (Ciotti et al., 1999). This result is not surprising because it is known that the shape of the

394 phytoplankton spectrum is affected both by the cell size of the major phytoplankton groups
395 and also by the intracellular pigment content (Morel and Bricaud, 1981).

396 *3.3.1 Impact of phytoplankton cell size on $a_{ph}^*(440)$* ---The importance of phytoplankton cell
397 size in determining $a_{ph}^*(440)$ is displayed in Figure 8, in which $a_{ph}^*(440)$ is plotted as a
398 function of the relative proportion in micro- (Fig. 8A), nano- (Fig. 8B), picophytoplankton
399 (Fig. 8C) and S_f (Fig. 8D). These relationships clearly show that the highest values of
400 $a_{ph}^*(440)$ are found within the surface layer and are associated with small phytoplankton cell
401 size (Fig. 8). We show that only 18% of the variability in $a_{ph}^*(440)$ could be attributed to the
402 microphytoplankton pool (mainly diatoms). The nanophytoplankton pool (prymnesiophytes
403 and pelagophytes) can explain 28% of the variability in $a_{ph}^*(440)$ and the picophytoplankton
404 pool (*Synechococcus sp.* and *Prochlorococcus sp.*) plays a significant role in changing
405 $a_{ph}^*(440)$, controlling 44 % of the variability (Fig. 8A, B, C). While we show that the S_f
406 parameter is not only dependent on the phytoplankton size but also on the intracellular
407 pigment content, we observe that S_f can explain 46% of the variation observed in $a_{ph}^*(440)$
408 (Fig. 8D). It is well established that phytoplankton functional types (PFTs) correspond to
409 phytoplankton species with similar biogeochemical roles and physiological traits and that the
410 phytoplankton size distribution is a major defining trait of PFTs (Le Quéré et al., 2005). The
411 size distribution is also known as a major factor determining particle sinking rates and thus
412 their role in carbon export (Eppley et al., 1967; McCave, 1975; Stemmann et al., 2004;
413 Buesseler et al., 2007). Therefore, in our study, we can considered that pico-, nano- and
414 microphytoplankton are three PFTs according to their size distribution. Thus, our results
415 confirm that variations in $a_{ph}(\lambda)$ can induce information about PFTs.

416 *3.3.2 Influence of changes in phytoplankton pigment composition on $a_{ph}^*(440)$* ---To examine
417 the impact of changes in phytoplankton pigments composition on $a_{ph}^*(440)$, we chose to
418 group the accessory phytoplankton pigments into four distinct categories: (1) [TChl b]; (2)

419 [TChl c]; (3) PSC and (4) PPC. The variability in $a_{ph}^*(440)$ as a function of the ratio of the
420 four categories of accessory pigments, relatively to [TChl *a*], is examined (Fig. 9). The [TChl
421 b]/[TChl *a*] ratio within the surface layer mainly varies in a narrow range from 0 to 0.25
422 while a broad range of variation in $a_{ph}^*(440)$ at depth can be observed (Fig. 9A), suggesting
423 that changes in proportion of chlorophyll b and divinyl chlorophyll b play no significant role
424 in the variability of $a_{ph}^*(440)$. The [TChl c]/[TChl *a*] ratio values vary from 0.03 to 0.35
425 (Fig. 9B) in all depths and from 0.03 to 0.18 within the surface layer. The increase in the
426 [TChl c]/[TChl *a*] ratio from 0 to 0.2 is accompanied by decreasing $a_{ph}^*(440)$ values (Fig.
427 9B). Some [TChl c]/[TChl *a*] values deviate from this trend, notably measurements collected
428 above the surface layer, for which the ratio is higher than 0.2. We show that only 24% of the
429 variability in $a_{ph}^*(440)$ could be associated with the [TChl c]/[TChl *a*] ratio (Fig. 9B). The
430 [PSC]/[TChl *a*] ratio mainly varies from 0.2 to 0.5 within as well above the surface while
431 $a_{ph}^*(440)$ show a more broad range of variations (Fig. 9C). The points where [PSC]/[TChl *a*]
432 ratio values are higher than 0.5 are the samples collected in the deeper layer. In many studies,
433 it has been shown that photosynthetic accessory pigment concentrations can increase with
434 increasing depth in response to lower light levels in deep waters (Bricaud and Stramski,
435 1990; Kirk, 1994; Majchrowski & Ostrowska, 2000). About 13% of the variability in
436 $a_{ph}^*(440)$ is attributed to the [PSC]/[TChl *a*] ratio. Unlike the [PSC]/[TChl *a*] ratio, the
437 [PPC]/[TChl *a*] ratio (mainly associated with zeaxanthin/[TChl *a*] in this study) varies in a
438 broad range from 0 to 1.2 (Fig. 9D). The highest [PPC]/[TChl *a*] values associated with
439 smaller phytoplankton cell size (S_f varying from 0.6 to 1) are observed within the surface
440 (Fig. 9D), and this is consistent with those observed in other oligotrophic regions
441 characterized by high light and low nutrient conditions (Bricaud et al., 1995, 2004; Stuart et
442 al., 1998, 2004, Barlow et al., 2004; Sathyendranath et al., 2005; Organelli et al., 2011).
443 Stuart et al. (2004) suggested that phytoplankton cells adapt to changes in light conditions

444 both by increasing their intracellular pigment content, and by changing the ratio of accessory
445 pigments. They noted that high concentrations of photoprotective pigments are a
446 characteristic feature of surface oligotrophic waters and can also be related to cell size. We
447 observe that an increase in the $[PPC]/[TChl\ a]$ ratio is accompanied by an increase in
448 $a_{ph}^*(440)$. About 51% of the variability in $a_{ph}^*(440)$ is due to the direct combined effect of
449 the $[PPC]/[TChl\ a]$ ratio and phytoplankton cell size, with the strongest contribution coming
450 from S_f , which explains 46% of the variability (Fig. 8D and 9D).

451 Summarizing the results in Figure 8 and 9, we notice that variations in phytoplankton cell
452 size as well as variations in $[PPC]/[TChl\ a]$ ratio are the main factors responsible for the
453 variability in $a_{ph}^*(440)$.

454 Figure 10 displays variations of SI and $[PPC]/[TChl\ a]$ ratio as a function of $[TChl\ a]$ for
455 diverse areas of the global ocean. As expected, the SI values increase with increasing $[TChl\ a]$
456 and are within the ranges of SI values found in various regions of the world's ocean,
457 although these measurements were restricted to the surface layer (Bricaud et al., 2004, 2010)
458 (Fig. 10A). On average, the phytoplankton community size structure seems to be slightly
459 smaller than those in the Mediterranean Sea and slightly larger than those in the Atlantic
460 Ocean (Fig. 10B). As reported in previous studies, the $[PPC]/[TChl\ a]$ ratio decrease
461 according to depth (higher values in surface water) in inverse relation to $[TChl\ a]$ (Bricaud et
462 al., 2004; Organelli et al., 2011). A group of low $[PPC]/[TChl\ a]$ values (> 0.2) is also
463 identified in the deeper layer and appears to not be related to $[TChl\ a]$ (Fig. 10C) as reported
464 in the Mediterranean Sea by Organelli et al. (2011). As for SI values, the $[PPC]/[TChl\ a]$
465 values are within the range of those observed in the other areas of the global ocean (Bricaud
466 et al., 2004, 2010). On average, the $[PPC]/[TChl\ a]$ values are slightly higher than those
467 observed in the Mediterranean Sea and in the Atlantic Ocean (Fig. 10D). Therefore, the
468 differences in average phytoplankton cell size and $[PPC]/[TChl\ a]$ values can affect the

469 variability in phytoplankton absorption and partially explain the higher $a_{ph}(\lambda)$ values at a
470 given [TChl *a*] observed in Red Sea waters compared to other areas of the global ocean.
471 Indeed, our results indicate that phytoplankton cell size associated to changes in PPC
472 pigments are rather well correlated to $a_{ph}^*(\lambda)$. The trend of decreasing cell size is associated
473 to an increase in [PPC]/[TChl *a*] ratio and $a_{ph}^*(\lambda)$ which is consistent with the expectation of
474 higher relative proportions of accessory pigments when the proportion of smaller
475 phytoplankton cells increases (Bricaud et al., 1995; Dupouy et al., 1997; Stuart et al., 1998,
476 2004). These results reflect the changes in phytoplankton community size structure in
477 response to the environmental conditions encountered in the Red Sea, which is characterized
478 as an oligotrophic region with high light and low nutrient concentrations. *Prochlorococcus*
479 and *Synechococcus* are known to be the most abundant organisms in highly stratified and
480 nutrient depleted oceans between 45° N and 45° S (Olson et al., 1990; Partensky et al., 1999;
481 Johnson et al., 2006; Al-Najjar et al., 2007; Shibl et al., 2014, 2016; Pearman et al., 2016;
482 Kheireddine et al., 2017). They correspond to phytoplankton of small size associated to a
483 high proportion in PPC pigments (mainly zeaxanthin pigment) which is consistent with our
484 observations in this study.

485

486 *3.4 Influence of environmental parameters on $a_{ph}^*(440)$* ---Recently, Kheireddine et al. (2017)
487 have suggested that latitudinal changes in physico-chemical variables, such as temperature
488 and salinity, may influence phytoplankton community size structure in Red Sea waters.
489 Temperature and salinity are known to be important environmental parameters that influence
490 phytoplankton community structure (Blanchot et al., 1992; Vaultot & Partensky, 1992;
491 Campbell & Vaultot, 1993; Veldhuis & Kraay, 1993; Moore et al., 1995; Ahel et al., 1996;
492 Graziano et al., 1996; Bouman et al., 2003, 2005; Lohrenz et al., 2003; Platt et al., 2005;
493 Loureiro et al., 2006; Hulyal and Kaliwal, 2009; Fehling et al., 2012). Thus, the variability

494 around the relationship between $a_{ph}^*(\lambda)$ and [TChl *a*] found in Red Sea waters might also be
495 associated with changes in physico-chemical conditions within the basin. In Figure 11,
496 $a_{ph}^*(440)$, temperature (T °C) and salinity are plotted as a function of the latitude. The spatial
497 distributions of $a_{ph}^*(440)$ and T °C showed similar latitudinal variations (Fig. 11A, B)
498 although no strong correlation is observed between $a_{ph}^*(440)$ and T °C (not shown). Both
499 parameters tend to increase from the SRS to the CRS and then to decrease from the CRS to
500 the NRS (Fig. 11A, B). The highest values of $a_{ph}^*(440)$ ($> 0.10 \text{ m}^2.\text{mg}^{-1}$) are, generally,
501 consistent with the highest values of T °C ($> 30^\circ\text{C}$) and high values of salinity (39-40.5) in
502 the CRS which is also the area where the abundance of picophytoplankton (mainly
503 *Prochlorococcus* and *Synechococcus sp.*) is the highest ($> 60 \%$ of the total phytoplankton
504 biomass) (Fig. 11A, B, C). This finding is consistent with observations in the Red Sea [Shibl
505 *et al.*, 2016; Kheiredine *et al.*, 2017] and from other oligotrophic regions (Partensky *et al.*,
506 1999; Bouman *et al.*, 2006; Zinzer *et al.*, 2007) where variations in temperature and salinity
507 influence the distribution of *Prochlorococcus* and *Synechococcus*. The lowest values of
508 $a_{ph}^*(440)$ are found in the two extremities of the basin where the proportions in bigger cells
509 to total phytoplankton biomass are higher than in the rest of the basin, as shown by
510 Kheireddine *et al.* (2017) based on HPLC measurements collected at the same period or
511 season (Fig. 11A).

512

513 **4. Conclusion**

514 We have shown that the absorption coefficients of phytoplankton and non-algal particles
515 measured in the Red Sea display a large variability associated with changes in environmental
516 conditions. This variability can affect the proportion of non-algal particles and the
517 phytoplankton community size structure. The cell size parameter and the proportion in the
518 [PPC]/[TChl *a*] ratio (mainly associated with zeaxanthin pigment) both play a key role in the

519 variability observed in $a_{ph}^*(440)$ (46 % and 51 %, respectively). Furthermore, values in $a_{ph}(\lambda)$
520 measured in this study are slightly higher for a given [TChl *a*] value than those estimated
521 from existing global relationships established for oligotrophic waters (Bricaud et al., 1995,
522 2004; Devred et al., 2006; Brewin et al., 2011), as well as for the Red Sea (Brewin et al.,
523 2015) within the first optical depth and among depths. These higher coefficients are
524 attributed to a higher relative proportion of PPC pigments, and smaller cell size. The
525 $a_{nap}(440)$ coefficients are also higher than those previously observed in oligotrophic waters
526 when [TChl *a*] < 0.1 mg.m⁻³ and lower when [TChl *a*] > 0.1 mg.m⁻³. In the clearest waters
527 ([TChl *a*] < 0.1 mg.m⁻³), the contribution of non-algal particles to total particulate absorption
528 was found to be higher than expected, suggesting the presence of more numerous inorganic
529 (dusts) and/or colored non-algal particles in these waters. Thus, in situ measurements to
530 quantify and identify these particles in the Red Sea waters including all environmental
531 conditions will be required.

532 It is known that some existing methods used to retrieve chlorophyll *a* needs to derive $a_{ph}(\lambda)$
533 from total light absorption and then estimate the chlorophyll *a* based on its relationship with
534 $a_{ph}(\lambda)$ (Garver and Siegel, 1997; Morel and Maritorena, 2001; Maritorena et al., 2002; Morel
535 et al., 2006). This relationship is essential for development of Red Sea algorithms for
536 estimating the diffuse attenuation coefficient of downward irradiance and ocean primary
537 production. Therefore, this study reveals the way to the refinement of ocean colour
538 algorithms to more accurately retrieve biogeochemical parameters (chlorophyll *a*
539 concentration, primary production, PFTs, etc.) in Red Sea waters.

540 **Acknowledgments**

541 The authors express their gratitude to the scientists, officers and crews of the research vessel
542 Thuwal and also the Coastal and Marine Resources Core Lab for logistical support and
543 assistance onboard during the fieldwork. U. Langner is cordially thanked for plotting the map
544 of the Red Sea, L. Solabarrieta and J. Otoadese for their advices and discussions on the
545 results presented here and for reading the manuscript. Alison Chase and the anonymous
546 reviewer are warmly thanked for the constructive comments on a previous version of the
547 manuscript. This study is funded by the King Abdullah University of Science and
548 Technology (KAUST), Kingdom of Saudi Arabia. The data presented in this study are
549 available from the authors upon request (malika.kheireddine@kaust.edu.sa) and are also
550 archived in <https://drive.google.com/open?id=0ByAL0hQpcGGPZmItRzh4eXNVdkk>.

551 **References**

- 552 Ahel, M., Barlow, R.G., & Mantoura, R.F.C. (1996). Effect of salinity gradients on the
553 distribution of phytoplankton pigments in a stratified estuary. *Marine Ecology Progress*
554 *Series*, 143 (1-3), 289-295. <https://doi.org/10.3354/meps143289>.
- 555 Al-Najjar, T., Badran, M.I., Richter, C., Meyerhoefer, M., & Sommer, U. (2007).
556 Seasonal dynamics of phytoplankton in the Gulf of Aqaba, Red Sea. *Hydrobiologia*, 579,
557 69-83. <https://doi.org/10.1007/s10750-006-0365-z>.
- 558 Al-Taani, A. A., Rashdan, M., & Khashashneh, S. (2015). Atmospheric dry deposition of
559 mineral dust to the Gulf of Aqaba, Red Sea: Rate and trace elements. *Marine Pollution*
560 *Bulletin*, 92 (1-2), 252-258. <https://doi.org/10.1016/j.marpolbul.2014.11.047>.
- 561 Allali, K., Bricaud, A., & Claustre, H. (1997). Spatial variations in the chlorophyll-
562 specific absorption coefficients of phytoplankton and photosynthetically active pigments
563 in the equatorial Pacific. *Journal of Geophysical Research-Oceans*, 102 (C6), 12413-
564 12423. <https://doi.org/10.1029/97JC00380>.

565 Almahasheer, H., Aljowair, A., Duarte, C. M., & Irigoien, X. (2016). Decadal stability of
566 Red Sea mangroves. *Estuarine Coastal and Shelf Sciences*, 169, 164-172.
567 <https://doi.org/10.1016/j.ecss.2015.11.027>.

568 Atlas, D., & Bannister, T. T. (1980). Dependence of mean spectral extinction coefficient
569 of phytoplankton on depth, water color, and species. *Limnology and Oceanography*, 25
570 (1), 157-159. <https://doi.org/10.4319/lo.1980.25.1.0157>.

571 Barlow, R., Kyewalyanga, M., Sessions, H., Van Den Berg, M., & Morris, T. (2008).
572 Phytoplankton pigments, functional types, and absorption properties in the Delagoa and
573 Natal Bights of the Agulhas ecosystem. *Estuarine Coastal and Shelf Sciences*, 80 (2),
574 201-211.

575 Barlow, R.G., Aiken, J.; Moore, G. F., Holligan, P. M. & Lavender, S. (2004). Pigment
576 adaptations in surface phytoplankton along the eastern boundary of the Atlantic Ocean.
577 *Marine Ecology Progress Series*, 281, 13-26. <https://doi.org/10.3354/meps281013> .

578 Belkin, I.M. (2009). Rapid warming of Large Marine Ecosystems. *Progress in*
579 *Oceanography*, 81 (1-4), 207-213. <https://doi.org/10.1016/j.pocean.2009.04.011>.

580 Berumen, M.L., Hoey, A., Bass, W., Bouwmeester, J., Catania, D., Cochran, J. E., Khalil,
581 M. T., Miyake, S., Mughal, M. R., & Spaet, J. (2013). The status of coral reef ecology
582 research in the Red Sea. *Coral Reefs*, 32 (3), 737-748. [https://doi.org/10.1007/s00338-](https://doi.org/10.1007/s00338-013-1055-8)
583 [013-1055-8](https://doi.org/10.1007/s00338-013-1055-8).

584 Blanchot, J., Rodier, M., & Leboutteiller, A. (1992). Effect of El-Niño southern oscillation
585 events on the distribution and abundance of phytoplankton in the western pacific tropical
586 ocean along 165° E. *Journal of Plankton Research*, 14 (1), 137-156.
587 <https://doi.org/10.1093/plankt/14.1.137>.

588 Boss, E., Gildor, H., Slade, W., Sokoletsky, L., Oren, A., & Loftin, J. (2013a). Optical
589 properties of the Dead Sea. *Journal of Geophysical Research-Oceans*, 118(4), 1821-
590 1829. <http://dx.doi.org/10.1002/jgrc.20109>.

591 Boss, E., Picheral, M., Leeuw, T., Chase, A., Karsenti, E., Gorsky, G., Taylor, L., Slade,
592 W., Ras, J., & Claustre, H. (2013b). The characteristics of particulate absorption,
593 scattering and attenuation coefficients in the surface ocean; Contribution of the Tara
594 Oceans expedition. *Method Oceanography*, 7, 52-62. [https://doi.org/
595 10.1016/j.mio.201311.002](https://doi.org/10.1016/j.mio.201311.002).

596 Boss, E.S., Collier, R., Larson, G., Fennel, K., & Pegau, S. W. (2007). Measurements of
597 spectral optical properties and their relation to biogeochemical variables and processes in
598 Crater Lake, Crater Lake National Park, OR. *Hydrobiologica*, 574, 149–1.
599 <https://doi.org/10.1007/s10750-006-2609-3>.

600

601 Bouman, H.A., Ulloa, O., Canlan, D.J., Zwirgmaier, K., Li, W.K.W., Platt, T., Stuart,
602 V., Barlow, R., Leth, O., Clementson, L., Lutz, V., Fukasawa, M., Watanabe, S., &
603 Sathyendranath, S. (2006). Oceanographic basis of the global surface distribution of
604 *Prochlorococcus* ecotypes. *Science*, 312 (5775), 918-921. [https://doi.org/
605 10.1126/science.1122692](https://doi.org/10.1126/science.1122692).

606 Bouman, H. A., Platt, T., Sathyendranath, S., & Stuart, V. (2005). Dependence of light-
607 saturated photosynthesis on temperature and community structure. *Deep Sea Research*, 52
608 (7), 1284-1299. [https://doi.org/ 10.1016/j.dsr.2005.01.008](https://doi.org/10.1016/j.dsr.2005.01.008).

609 Bouman, H.A., Platt, T., Sathyendranath, S., Li, W. K. W., Stuart, V., Fuentes-Yaco, C.,
610 Maass, H., Horne, E.P.W., Ulloa, O., Lutz, V., & Kyewalyanga, M. (2003). Temperature
611 as indicator of optical properties and community structure of marine phytoplankton:

612 implications for remote sensing. *Marine Ecology Progress Series*, 258, 19-30.
613 [https://doi.org/ 10.3354/meps258019](https://doi.org/10.3354/meps258019).

614 Bracher A., Bouman, H.A, Brewin, R.J.W., Bricaud, A., Brotas, V., Ciotti, A.M.,
615 Clementson, L., Devred, E., Di Cicco, A., Dutkiewicz, S., Hardman-Mountford, N.J.,
616 Hickman, A.E., Hieronymi, M., Hirata, T., Losa, S.N., Mouw, C.B., Organelli, E.,
617 Raitzos, D.E., Uitz, J., Vogt, M., & Wolanin, A. (2017). Obtaining Phytoplankton
618 Diversity from Ocean Color: A Scientific Roadmap for Future Development. *Frontiers in*
619 *Marine Sciences*, 4:55. <https://doi.org/10.3389/fmars.2017.00055>

620 Brewin, R.J.W., Raitzos, D.E., Dall'Olmo, G., Zarokanellos, N., Jackson, T., Racault,
621 M.-F., Boss, E., Sathyendranath, S., Jones, B.H., & Hoteit, I. (2015). Regional ocean-
622 colour chlorophyll algorithms for the Red Sea. *Remote Sensing Environment*, 165, 64-85.
623 [https://doi.org/ 10.1016/j.rse.2015.04.024](https://doi.org/10.1016/j.rse.2015.04.024).

624 Brewin, R.J.W., Devred, E., Sathyendranath, S., Lavender, S.J., & Hardman-Mountford,
625 N. J. (2011). Model of phytoplankton absorption based on three size classes. *Applied*
626 *Optics*, 50 (22), 4535-4549. [https://doi.org/ 10.1364/AO.50.004535](https://doi.org/10.1364/AO.50.004535).

627 Bricaud, A., Babin, M., Claustre, H., Ras, J., & Tieche, F. (2010). Light absorption
628 properties and absorption budget of Southeast Pacific waters. *Journal of Geophysical*
629 *Research-Oceans*, 115, C08009. [https://doi.org/ 10.1029/2009JC005517](https://doi.org/10.1029/2009JC005517).

630 Bricaud, A., Claustre, H., Ras, J., & Oubelkheir, K. (2004). Natural variability of
631 phytoplanktonic absorption in oceanic waters: Influence of the size structure of algal
632 populations. *Journal of Geophysical Research*, 109 (C11). [https://doi.org/](https://doi.org/10.1029/2004JC002419)
633 [10.1029/2004JC002419](https://doi.org/10.1029/2004JC002419).

634 Bricaud, A., Morel, A., Babin, M., Allali, K., & Claustre, H. (1998). Variations of light
635 absorption by suspended particles with chlorophyll a concentration in oceanic (case 1)

636 waters: Analysis and implications for bio-optical models. *Journal of Geophysical*
637 *Research*, 103 (C13), 31033-31044. [https://doi.org/ 10.1029/98JC02712](https://doi.org/10.1029/98JC02712).

638 Bricaud, A., Babin, M., Morel, A., & Claustre, H. (1995). Variability in the chlorophyll-
639 specific absorption coefficients of natural phytoplankton: Analysis and parameterization.
640 *Journal of Geophysical Research-Oceans*, 100 (C7), 13321-13332, [https://doi.org/](https://doi.org/10.1029/95JC00463)
641 [10.1029/95JC00463](https://doi.org/10.1029/95JC00463).

642 Bricaud, A., & Morel, A. (1986). light attenuation and scattering bt phytoplanktonic cells:
643 Atheoretical modeling. *Applied Optics*, 25 (4), 571-580.

644 Bricaud, A., & Stramski, D. (1990). Spectral absorption coefficients of living
645 phytoplankton and nonalgal biogenous matter: A comparison between the Peru upwelling
646 area and the Sargasso Sea. *Limnology and Oceanography*, 35 (3), 562-582.
647 [https://doi.org/ 10.4319/lo.1990.35.3.0562](https://doi.org/10.4319/lo.1990.35.3.0562).

648 Brunelle, C.B., Larouche, P., & Gosselin, M. (2012). Variability of phytoplankton light
649 absorption in Canadian Arctic seas. *Journal of Geophysical Research-Oceans*, 117, C9.
650 [https://doi.org/ 10.1029/2011JC007345](https://doi.org/10.1029/2011JC007345).

651 Buesseler, K. O., Lamborg, C. H., Boyd, P. W., Lam, P. J., Trull, T.W., Bidigare, R. R.,
652 Bishop, J. K. B., Casciotti, K. L., Dehairs, F., Elskens, M., Honda, M., Karl, D. M.,
653 Siegel, D. A., Silver, M. W., Steinberg, D. K., Valdes, J. B., Mooy, B. V., & Wilson, S.
654 (2007). Revisiting Carbon Flux through the Ocean's Twilight Zone. *Science*, 316, 567–
655 570.

656 Campbell, L., & Vaultot, D. (1993). Photosynthetic picoplankton community struture in
657 the subtropical North Pacific Ocean near Hawaii (station ALOHA). *Deep Sea Research*,
658 40 (10), 2043-2060. [https://doi.org/ 10.1016/0967-0637\(93\)90044-4](https://doi.org/10.1016/0967-0637(93)90044-4).

659 Churchill, J.H., Bower, A.S., McCorkle, D.C., Abualnaja, Y. (2014), The transport of
660 nutrient-rich Indian Ocean water through the Red Sea and into coastal reef systems.

661 *Journal of Marine Research*, 72 (3), 165-181. [https://doi.org/](https://doi.org/10.1357/002224014814901994)
662 10.1357/002224014814901994.

663 Ciotti, A.M., & Bricaud, A. (2006). Retrievals of a size parameter for phytoplankton and
664 spectral light absorption by colored detrital matter from water-leaving radiances at
665 SeaWiFS channels in a continental shelf region off Brazil. *Limnology and Oceanography*
666 *Methods*, 4, 237-253. [https://doi.org/ 10.4319/lom.2006.4.237](https://doi.org/10.4319/lom.2006.4.237).

667 Ciotti, A.M., Lewis, M. R., & Cullen, J. J. (2002). Assessment of the relationships
668 between dominant cell size in natural phytoplankton communities and the spectral shape
669 of the absorption coefficient. *Limnology and Oceanography*, 47 (2), 404-417.
670 [https://doi.org/ 10.4319/lo.2002.47.2.0404](https://doi.org/10.4319/lo.2002.47.2.0404).

671 Ciotti, A.M., Cullen, J.J., & Lewis, M. R. (1999). A semi-analytical model of the
672 influence of phytoplankton community structure on the relationship between light
673 attenuation and ocean color. *Journal of Geophysical Research*, 104 (C1), 1559-1578.
674 [https://doi.org/ 10.1029/1998JC900021](https://doi.org/10.1029/1998JC900021).

675 Cleveland, J.S. (1995). Regional models for phytoplankton absorption as a function of
676 chlorophyll a concentration. *Journal of Geophysical Research*, 100 (C7), 13333-13344.
677 [https://doi.org/ 10.1029/95JC00532](https://doi.org/10.1029/95JC00532).

678 Dall'Olmo, G., Boss, E., Behrenfeld, M. J., & Westberry, T. K. (2012). Particulate optical
679 scattering coefficients along an Atlantic Meridional Transect. *Optics Express*, 20 (19),
680 21532-21551. [https://doi.org/ 10.1364/OE.20.021532](https://doi.org/10.1364/OE.20.021532).

681 Dall'Olmo, G., Westberry, T. K., Behrenfeld, M. J., Boss, E., & Slade, W. H. (2009).
682 Significant contribution of large particles to optical backscattering in the open ocean.
683 *Biogeosciences*, 6 (6), 947-967. [https://doi.org/ 10.5194/bg-6-947-2009](https://doi.org/10.5194/bg-6-947-2009).

684 Devred, E., Sathyendranath, S., Stuart, V., Maass, H., Ulloa, O., & Platt, T. (2006). A
685 two-component model of phytoplankton absorption in the open ocean: Theory and

686 applications. *Journal of Geophysical Research*, 111 (C3), 2156-2202. [https://doi.org/](https://doi.org/10.1029/2005JC002880)
687 10.1029/2005JC002880.

688 Dreano, D., Raitzos, D.E., Gittings, J., Krokos, G., & Hoteit I. (2016), The Gulf of Aden
689 Intermediate Water Intrusion Regulates the Southern Red Sea Summer Phytoplankton
690 Blooms, *Plos One*, 11 (12),. [https://doi.org/ 10.1371/journal.pone.0168440](https://doi.org/10.1371/journal.pone.0168440).

691 Dupouy, C., Neveux, J., & Andre, J. M. (1997). Spectral absorption coefficient of
692 photosynthetically active pigments in the equatorial Pacific Ocean (165 °E-150 °W).
693 *Deep Sea Research*, 44 (9-10), 1881-1906. [https://doi.org/ 10.1016/S0967-](https://doi.org/10.1016/S0967-0645(97)00078-7)
694 0645(97)00078-7.

695 Eppley, R. W., Holmes, R. W., & Strickland II., J. D. (1967). Sinking rates of marine
696 phytoplankton measured with a fluorometer. *Journal of Experimental Marine Biology*
697 *and Ecology*, 1, 191–208. [https://doi.org/10.1016/0022-0981\(67\)90014-7](https://doi.org/10.1016/0022-0981(67)90014-7).

698 Fehling, J., Davidson, K., Bolch, C.J.S., Brand, T. D., & Narayanaswamy, B. E. (2012).
699 The Relationship between Phytoplankton Distribution and Water Column Characteristics
700 in North West European Shelf Sea Waters. *Plos One*, 7 (3).
701 <https://doi.org/10.1371/journal.pone.0034098>.

702 Ferreira, A., Stramski, D., Garcia, C.A.E., Garcia, V.M.T., Ciotti, A. M., & Mendes, C.
703 R. B. (2013). Variability in light absorption and scattering of phytoplankton in Patagonian
704 waters: Role of community size structure and pigment composition. *Journal of*
705 *Geophysical Research*, 118 (2), 698-714. [https://doi.org/ 10.1002/jgrc.20082](https://doi.org/10.1002/jgrc.20082).

706 Garver, S.A., & Siegel, D. A. (1997). Inherent optical property inversion of ocean color
707 spectra and its biogeochemical interpretation .1. Time series from the Sargasso Sea.
708 *Journal of Geophysical Research*, 102 (C8), 18607-18625. [https://doi.org/](https://doi.org/10.1029/96JC03243)
709 10.1029/96JC03243.

710 Ginoux, P., Prospero, J.M., Gill, T.E., Hsu, N.C., Zhao, M. (2012). Global-scale
711 attribution of anthropogenic and natural dust sources and their emission rates based on
712 MODIS Deep Blue aerosol products. *Reviews of Geophysics*, 50 (3), 1944-9203.
713 [https://doi.org/ 10.1029/2012RG000388](https://doi.org/10.1029/2012RG000388).

714 Gittings, J.A., Raitsos, D.E., Racault, M-F., Brewin, R.J., Pradhan, Y., Sathyendranath, S.,
715 Platt, T. (2017). Seasonal Phytoplankton Blooms in the Gulf of Aden revealed by Remote
716 Sensing. *Remote Sensing Environment*, 189 (2017), 56–66.
717 <http://dx.doi.org/10.1016/j.rse.2016.10.043>.

718 Gordon, H.R., & McCluney, W.R. (1975). Estimation of the depth of sunlight penetration
719 in the sea for remote sensing. *Applied Optics*, 14(2), 413-416.
720 <http://dx.doi.org/10.1364/ao.14.000413>.

721 Graziano, L.M., Geider, R.J., Li, W.K.W., & Olaizola, M. (1996). Nitrogen limitation of
722 North Atlantic phytoplankton: Analysis of physiological condition in nutrient enrichment
723 experiments. *Aquatic Microbial Ecology*, 11 (1), 53-64. [https://doi.org/](https://doi.org/10.3354/ame011053)
724 [10.3354/ame011053](https://doi.org/10.3354/ame011053).

725 Hulyal, S.B., & Kaliwal, B. B. (2009). Dynamics of phytoplankton in relation to physico-
726 chemical factors of Almatti reservoir of Bijapur District, Karnataka State. *Environmental*
727 *Monitoring and Assessment*, 153 (1-4), 45-59. [https://doi.org/ 10.1007/s10661-008-0335-](https://doi.org/10.1007/s10661-008-0335-1)
728 [1](https://doi.org/10.1007/s10661-008-0335-1).

729 Ismael, A. A. (2015). Phytoplankton of the Red Sea. In *The Red Sea* (pp. 567-583).
730 Springer Berlin Heidelberg.

731 Johnson, Z.I., Zinser, E.R., Coe, A., McNulty, N.P., Woodward, E.M.S., & Chisholm,
732 S.W. (2006). Niche partitioning among *Prochlorococcus* ecotypes along ocean-scale
733 environmental gradients. *Science*, 311 (5768), 1737-1740. [https://doi.org/](https://doi.org/10.1126/science.1118052)
734 [10.1126/science.1118052](https://doi.org/10.1126/science.1118052).

735 Kheireddine, M., Ouhssain, M., Claustre, H., Uitz J., Gentili, B., & Jones, B.H. (2017).
736 Assessing Pigment-Based Phytoplankton Community Distributions in the Red Sea.
737 *Frontiers in Marine Science*, 4, 2296-7745. [https://doi.org/ 10.3389/fmars.2017.00132](https://doi.org/10.3389/fmars.2017.00132).

738 Kiefer, D.A., & Mitchell, B. G. (1983). A simple, steady-state description of
739 phytoplankton growth based on absorption cross-section and quantum efficiency.
740 *Limnology and Oceanography*, 28 (4), 770-776. [https://doi.org/](https://doi.org/10.4319/lo.1983.28.4.0770)
741 [10.4319/lo.1983.28.4.0770](https://doi.org/10.4319/lo.1983.28.4.0770).

742 Kirk, J.T. (1994), Light and photosynthesis in aquatic ecosystems, Cambridge university
743 press. 401 pp.

744 Kishino, M., Takahashi, M., Okami, N., & Ichimura, S. (1985), Estimation of the spectral
745 absorption coefficients of phytoplankton in the Sea. *Bulletin of Marine Science*, 37 (2),
746 634-642.

747 Lekunberri, I., Lefort, T., Romero, E., Vazquez-Dominguez, E., Romera-Castillo, C.,
748 Marrase, C., Peters, F., Weinbauer, M., Gasol, J.M. (2010). Effects of a dust deposition
749 event on coastal marine microbial abundance and activity, bacterial community structure
750 and ecosystem function. *Journal of Plankton Research*, 32 (4), 381-396. [https://doi.org/](https://doi.org/10.1093/plankt/fbp137)
751 [10.1093/plankt/fbp137](https://doi.org/10.1093/plankt/fbp137).

752 Le Quéré, C., et al. (2005). Ecosystem dynamics based on plankton functional types for
753 global ocean biogeochemistry models. *Global Change Biology*, 11(11), 2016-2040.
754 <https://doi.org/10.1111/j.1365-2468.2005.01004.x>.

755 Lohrenz, S.E., Weidemann, A. D., & Tuel, M. (2003). Phytoplankton spectral absorption
756 as influenced by community size structure and pigment composition. *Journal of Plankton*
757 *Research*, 25 (1), 35-61. [https://doi.org/ 10.1093/plankt/25.1.35](https://doi.org/10.1093/plankt/25.1.35).

758 Longhurst, A. (2007). Toward an ecological geography of the sea. *Ecological Geography*
759 *of the Sea*, 1-17.

760 Loureiro, S., Newton, A., & Icely, J. (2006). Boundary conditions for the European water
761 framework directive in the ria Formosa lagoon, Portugal (physico-chemical and
762 phytoplankton quality elements). *Estuarine, Coastal and Shelf Science*, 67 (3), 382-398.
763 [https://doi.org/ 10.1016/j.ecss.2005.11.029](https://doi.org/10.1016/j.ecss.2005.11.029).

764 Lutz, V.A., Sathyendranath, S., & Head, E. J. H. (1996). Absorption coefficient of
765 phytoplankton: Regional variations in the North Atlantic. *Marine Ecology Progress
766 Series*, 135 (1-3), 197-213. [https://doi.org/ 10.3354/meps135197](https://doi.org/10.3354/meps135197).

767 Majchrowski R., & Ostrowska, M. (2000). Influence of photo- and chromatic
768 acclimation on pigment composition in the sea. *Oceanologia*, 42(2), 157–175.
769 [https://doi.org/ 10.1029/2002JD002536](https://doi.org/10.1029/2002JD002536).

770 Maritorena, S., Siegel, D. A., & Peterson, A. R., (2002). Optimization of a semianalytical
771 ocean color model for global-scale applications. *Applied Optics*, 41 (15), 2705-2714.
772 [https://doi.org/ 10.1364/AO.41.002705](https://doi.org/10.1364/AO.41.002705).

773 McCave, I. N. (1975). Vertical flux of particles in the ocean. *Deep Sea Research*,
774 22(7), 491–502.

775 Mitchell, B.G., & Kiefer, D. A. (1988). Variability in pigment specific particulate
776 fluorescence and absorption spectra in the northeastern Pacific Ocean. *Deep Sea
777 Research*, 35 (5), 665-689.

778 Mitchell, B.G., Kahru, M., Wieland, J., & Stramska, M. (2003). Determination of spectral
779 absorption coefficients of particles, dissolved material and phytoplankton for discrete
780 water samples. In: Mueller, J.L., G.S. Fargion, and C.R. McClain [Eds.] *Ocean Optics
781 Protocols for Satellite Ocean Color Sensor Validation, Revision 4, Volume IV: Inherent
782 Optical*.

783 Moore, L.R., Goericke, R., & Chisholm, S. W. (1995). Comparative physiology of
784 *Synechococcus* and *Prochlorococcus* : Influence of light and temperature on growth,

785 pigments, fluorescence and absorptive properties. *Marine Ecology Progress Series*, 116
786 (1-3), 259-275.

787 Morales-Baquero, R., Pulido-Villena, E., Reche, I. (2013). Chemical signature of Saharan
788 dust on dry and wet atmospheric deposition in the south-western Mediterranean region.
789 *Tellus B*, 65. [https://doi.org/ 10.3402/tellusb.v65i0.18720](https://doi.org/10.3402/tellusb.v65i0.18720).

790 Morel, A. (1991). Light and marine photosynthesis: A spectral model with geochemical
791 and climatological implications. *Progress in Oceanography*, 26 (3), 263-306.
792 [https://doi.org/ 10.1016/0079-6611\(91\)90004-6](https://doi.org/10.1016/0079-6611(91)90004-6).

793 Morel, A., & Bricaud, A. (1981). Theoretical results concerning light absorption in a
794 discrete medium, and application to specific absorption of phytoplankton. *Deep Sea*
795 *Research*, 28 (11), 1375-1393.

796 Morel, A., Huot, Y., Gentili, B., Werdell, P. J., Hooker, S.B., & Franz, B. A. (2007).
797 Examining the consistency of products derived from various ocean color sensors in open
798 ocean (Case 1) waters in the perspective of a multi-sensor approach. *Remote Sensing*
799 *Environment*, 111 (1), 69-88. [https://doi.org/ 10.1016/j.rse.2007.03.012](https://doi.org/10.1016/j.rse.2007.03.012).

800 Morel, A., Gentili, B., Chami, M. & Ras, J. (2006). Bio-optical properties of high
801 chlorophyll Case 1 waters and of yellow-substance-dominated Case 2 waters. *Deep Sea*
802 *Research*, 53 (9), 1439-1459, [https://doi.org/ 10.1016/j.dsr.2006.07.007](https://doi.org/10.1016/j.dsr.2006.07.007).

803 Morel, A., & Maritorena, S. (2001). Bio-optical properties of oceanic waters: A
804 reappraisal. *Journal of Geophysical Research*, 106 (C4), 7163-7180. [https://doi.org/](https://doi.org/10.1029/2000JC000319)
805 [10.1029/2000JC000319](https://doi.org/10.1029/2000JC000319).

806 Neumann, A.C., McGill, D.A. (1962). Circulation of the Red Sea in early summer. *Deep*
807 *Sea Research*, 8 ((3/4)), 223-235.

808 Olson, R.J., Chisholm, S.W., Zettler, E.R., & Armbrust, E. V. (1990). Pigments, size, and
809 distribution of *Synechococcus* in the North Atlantic and Pacific Oceans. *Limnology and*
810 *Oceanography*, 35 (1), 45-58. [https://doi.org/ 10.4319/lo.1990.35.1.0045](https://doi.org/10.4319/lo.1990.35.1.0045).

811 Organelli, E., Claustre, H., Bricaud, A., Barbieux, M., Uitz, J., D'Ortenzio, F. &
812 Dall'Olmo, G. (2017). Bio-optical anomalies in the world's oceans: an investigation on
813 the diffuse light attenuation coefficients derived from Biogeochemical Argo float
814 measurements. *Journal of Geophysical Research*, 122. [https://doi.org/](https://doi.org/10.1002/2016JC012629)
815 [10.1002/2016JC012629](https://doi.org/10.1002/2016JC012629).

816

817 Organelli, E., Bricaud, A., Antoine, D., Matsuoka, A. (2014). Seasonal dynamics of light
818 absorption by chromophoric dissolved organic matter (CDOM) in the NW Mediterranean
819 Sea (BOUSSOLE site). *Deep Sea Research*, 91, 72-85.
820 <https://doi.org/10.1016/j.dsr.2014.05.003>.

821 Organelli, E., Bricaud, A., Antoine, D., & Uitz, J. (2013). Multivariate approach for the
822 retrieval of phytoplankton size structure from measured light absorption spectra in the
823 Mediterranean Sea (BOUSSOLE site). *Applied Optics*, 52 (11), 2257-2273.
824 [https://doi.org/ 10.1364/AO.52.002257](https://doi.org/10.1364/AO.52.002257).

825 Organelli, E., Nuccio, C., Melillo, C., & Massi, L. (2011). Relationships between
826 phytoplankton light absorption, pigment composition and size structure in offshore areas
827 of the Mediterranean Sea. *Advances in Oceanography and Limnology*, 2(2), 107-123.
828 [https://doi.org/ 10.1080/19475721.2011.607489](https://doi.org/10.1080/19475721.2011.607489).

829 Partensky, F., Hess, W. R., & Vaulot, D. (1999). Prochlorococcus, a marine
830 photosynthetic prokaryote of global significance. *Microbiology and Molecular Biology*
831 *Reviews*, 63 (1), 106-+.

832 Partensky, F., LaRoche, J., Wyman, K., & Falkowski, P. G. (1997). The divinyl-
833 chlorophyll a/b-protein complexes of two strains of the oxyphototrophic marine
834 prokaryote *Prochlorococcus* - Characterization and response to changes in growth
835 irradiance. *Photosynthesis Research*, 51 (3), 209-222. [https://doi.org/](https://doi.org/10.1023/A:1005807408161)
836 10.1023/A:1005807408161.

837 Patzert, W.C. (1974), Wind-induced reversal in Red Sea circulation. *Deep Sea Research*,
838 21 (2), 109-121.

839 Pearman, J.K., Kurten, S., Sarma, Y. V. B., Jones, B. H. & Carvalho, S. (2016),
840 Biodiversity patterns of plankton assemblages at the extremes of the Red Sea. *FEMS*
841 *microbiology Ecology*, 92 (3). [https://doi.org/ 10.1093/femsec/fiw002](https://doi.org/10.1093/femsec/fiw002).

842 Perez, G., Queimalinos, C., Balseiro, E., & Modenutti, B. (2007). Phytoplankton
843 absorption spectra along the water column in deep North Patagonian Andean lakes
844 (Argentina). *Limnologica* ,37 (1), 3-16. [https://doi.org/ 10.1016/j.limno.2006.08.005](https://doi.org/10.1016/j.limno.2006.08.005).

845 Platt, T., Bouman, H., Devred, E., Fuentes-Yaco, C., & Sathyendranath, S. (2005).
846 Physical forcing and phytoplankton distributions. *Scientia Marina*, 69, 55-73.

847 Platt, T., & Sathyendranath, S. (1988). Oceanic primary production: Estimation by remote
848 sensing at local and regional scales. *Science*, 241 (4873), 1613-1620. [https://doi.org/](https://doi.org/10.1126/science.241.4873.1613)
849 10.1126/science.241.4873.1613.

850 Ploug, H., Iversen, M. H., & Fisher, G. (2008). Ballast Sinking velocity, and apparent
851 diffusivity within marine snow and zooplankton fecal pellets: implications for substrate
852 turnover by attached bacteria. *Limnology and Oceanography*, 53, 1878–1886.

853 Prakash, P.J., Stenchikov, G., Kalenderski, S., Osipov, S., Bangalath, H. (2015). The
854 impact of dust storms on the Arabian Peninsula and the Red Sea. *Atmospheric Chemistry*
855 *and Physics*, 15 (1), 199-222. [https://doi.org/ 10.5194/acp-15-199-2015](https://doi.org/10.5194/acp-15-199-2015).

856 Prospero, J.M., Ginoux, P., Torres, O., Nicholson, S.E., Gill, T.E. (2002). Environmental
857 characterization of global sources of atmospheric soil dust identified with the Nimbus 7
858 Total Ozone Mapping Spectrometer (TOMS) absorbing aerosol product. *Reviews*
859 *Geophysics*, 40 (1). [https://doi.org/ 10.1029/2000rg000095](https://doi.org/10.1029/2000rg000095).

860 Racault, M.-F., Raitzos, D.E., Berumen, M.L., Brewin, R.J.W., Platt, T.,
861 Sathyendranath, S., & Hoteit, I. (2015). Phytoplankton phenology indices in coral reef
862 ecosystems: Application to ocean-color observations in the Red Sea. *Remote Sensing*
863 *Environment*, 160, 222-234. <https://doi.org/10.1016/j.rse.2015.01.019>.

864 Raitzos, D.E., Yi, X., Platt, T., Racault, M.-F., Brewin, R.J.W., Pradhan, Y.,
865 Papadopoulos, V.P., Sathyendranath, S., & Hoteit, I. (2015). Monsoon oscillations
866 regulate fertility of the Red Sea. *Geophysical Research Letters*, 42 (3), 855-862.
867 <https://doi.org/10.1002/2014GL062882>.

868 Raitzos, D.E., Pradhan, Y., Brewin, R.J.W., Stenchikov, G., & Hoteit, I. (2013). Remote
869 Sensing the Phytoplankton Seasonal Succession of the Red Sea. *Plos One*, 8 (6).
870 [https://doi.org/ 10.1371/journal.pone.0064909](https://doi.org/10.1371/journal.pone.0064909).

871 Raitzos, D.E., Hoteit, I., Prihartato, P.K., Chronis, T., Triantafyllou, G., & Abualnaja, Y.
872 (2011). Abrupt warming of the Red Sea. *Geophysical Research Letters*, 38.
873 [https://doi.org/ 10.1029/2011GL047984](https://doi.org/10.1029/2011GL047984).

874 Ras, J., Claustre, H., & Uitz, J. (2008). Spatial variability of phytoplankton pigment
875 distributions in the Subtropical South Pacific Ocean: comparison between in situ and
876 predicted data. *Biogeosciences*, 5 (2), 353-369. [https://doi.org/ 10.5194/bg-5-353-2008](https://doi.org/10.5194/bg-5-353-2008).

877 Reche, I., Ortega-Retuerta, E., Romera, O., Pulido-Villena, E., Morales-Baquero, R.,
878 Casamayor, E.O. (2009). Effect of Saharan dust inputs on bacterial activity and
879 community composition in Mediterranean lakes and reservoirs. *Limnology and*
880 *Oceanography*, 54 (3), 869-879. [https://doi.org/ 10.4319/lo.2009.54.3.0869](https://doi.org/10.4319/lo.2009.54.3.0869).

881 Roesler, C. S. & Barnard, A. H. (2013). Optical proxy for phytoplankton biomass in the
882 absence of photophysiology: Rethinking the absorption line height. *Methods in*
883 *Oceanography*, 7: 79-94. [https://doi.org/ 10.1016/j.mio.2013.12.003](https://doi.org/10.1016/j.mio.2013.12.003).

884 Roesler, C. S., & Perry, M. J. (1995). In situ phytoplankton absorption, fluorescence
885 emission, and particulate backscattering spectra determined from reflectance. *Journal of*
886 *Geophysical Research*, 100 (C7), 13279-13294. [https://doi.org/ 10.1029/95JC00455](https://doi.org/10.1029/95JC00455).

887 Roy, S., Sathyendranath, S. & Platt, T. (2011). Retrieval of phytoplankton size from bio-
888 optical measurements: theory and applications. *Journal of The Royal Society Interface*, 8
889 (58), 650-660. [https://doi.org/ 10.1098/rsif.2010.0503](https://doi.org/10.1098/rsif.2010.0503).

890 Sathyendranath, S., Stuart, V., Platt, T., Bouman, H., Ulloa, O., & Maass, H. (2005).
891 Remote sensing of ocean colour: Towards algorithms for retrieval of pigment
892 composition. *Indian Journal of Marine Sciences*, 34 (4), 333-340.

893 Sathyendranath, S., Cota, G., Stuart, V., Maass, H., & Platt, T. (2001). Remote sensing of
894 phytoplankton pigments: a comparison of empirical and theoretical approaches.
895 *International Journal of Remote Sensing*, 22 (2-3), 249-273. [https://doi.org/](https://doi.org/10.1080/014311601449925)
896 [10.1080/014311601449925](https://doi.org/10.1080/014311601449925).

897 Sathyendranath, S., Stuart, V., Irwin, B.D., Maass, H., Savidge, G., Gilpin, L. & Platt, T.
898 (1999). Seasonal variations in bio-optical properties of phytoplankton in the Arabian Sea,
899 *Deep Sea Research*, 46 (3-4), 633-653. [https://doi.org/ 10.1016/S0967-0645\(98\)00121-0](https://doi.org/10.1016/S0967-0645(98)00121-0).

900 Sathyendranath, S., Platt, T., Stuart, V., Irwin, B.D., Veldhuis, M.J.W., Kraay, G.W., &
901 Harrison, W. G. (1996). Some bio-optical characteristics of phytoplankton in the NW
902 Indian Ocean. *Marine Ecology Progress Series*, 132 (1-3), 299-311.

903 Sathyendranath, S., Lazzara, L. & Prieur, L. (1987). Variations in the spectral values of
904 specific absorption of phytoplankton. *Limnology and Oceanography*, 32 (2), 403-415.

905 Sathyendranath, S., & Platt, T. (1988). The spectral irradiance field at the surface and in
906 the interior of the ocean: A model for applications in oceanography and remote sensing.
907 *Journal of Geophysical Research*, 93 (C8), 9270-9280. [https://doi.org/](https://doi.org/10.1029/JC093iC08p09270)
908 10.1029/JC093iC08p09270.

909 Sawall, Y., Al-Sofyani, A., Banguera-Hinestroza, E., & Voolstra, C. R. (2014). Spatio-
910 temporal analyses of Symbiodinium physiology of the coral *Pocillopora verrucosa* along
911 large-scale nutrient and temperature gradients in the Red Sea. *PloS one*, 9(8), e103179.

912 Shibl, A.A., Haroon, M.F., Ngugi, D.K., Thompson, L.R., & Stingl, U. (2016).
913 Distribution of *Prochlorococcus* Ecotypes in the Red Sea Basin Based on Analyses of
914 rpoC1 Sequences. *Frontiers in Marine Science*, 3 (104). [https://doi.org/](https://doi.org/10.3389/fmars.2016.00104)
915 10.3389/fmars.2016.00104.

916 Shibl, A.A., Thompson, L.R., Ngugi, D.K., & Stingl, U. (2014). Distribution and
917 diversity of *Prochlorococcus* ecotypes in the Red Sea. *FEMS microbiology letters*, 356
918 (1), 118-126. [https://doi.org/ 10.1111/1574-6968.12490](https://doi.org/10.1111/1574-6968.12490).

919 Sofianos, S.S., & Johns W.E. (2007), Observations of the summer red sea circulation.
920 *Journal of Geophysical Research*, 112 (C6), 1-20. [https://doi.org/](https://doi.org/10.1029/2006JC003886)
921 10.1029/2006JC003886.

922 Sofianos, S.S., & Johns, W.E. (2003). An Oceanic General Circulation Model (OGCM)
923 investigation of the Red Sea circulation: 2. Three-dimensional circulation in the Red Sea.
924 *Journal of Geophysical Research*, 108 (C3). [https://doi.org/ 10.1029/2001JC001184](https://doi.org/10.1029/2001JC001184),
925 2002.

926 Stemmann, L., Jackson, G. A., & Ianson, D. (2004). A vertical model of particle size
927 distributions and fluxes in the midwater column that includes biological and
928 physical processes – Part I: model formulation,. *Deep Sea Research*, 51(7), 865–
929 884. <https://doi.org/10.1016/j.dsr.2004.03.001>.

930 Stramski, D., Reynolds, R.A., Kaczmarek, S., Uitz, J., & Zheng, G. M. (2015).
931 Correction of pathlength amplification in the filter-pad technique for measurements of
932 particulate absorption coefficient in the visible spectral region. *Applied Optics*, 54 (22),
933 6763-6782. [https://doi.org/ 10.1364/AO.54.006763](https://doi.org/10.1364/AO.54.006763).

934 Stuart, V., Ulloa, O., Alarcon, G., Sathyendranath, S., Major, H., Head, E.J.H., & Platt, T.
935 (2004). Bio-optical characteristics of phytoplankton populations in the upwelling system
936 off the coast of Chile. *Revista Chilena De Historia Natural*, 77 (1), 87-105.
937 [https://doi.org/ 10.4067/S0716-078X2004000100008](https://doi.org/10.4067/S0716-078X2004000100008).

938 Stuart, V., Sathyendranath, S., Platt, T., Maass, H., & Irwin, B. D. (1998). Pigments and
939 species composition of natural phytoplankton populations: effect on the absorption
940 spectra. *Journal of Plankton Research*, 20 (2), 187-217. [https://doi.org/](https://doi.org/10.1093/plankt/20.2.187)
941 [10.1093/plankt/20.2.187](https://doi.org/10.1093/plankt/20.2.187).

942 Suzuki, K., Kishino, M., Sasaoka, K., Saitoh, S., & Saino, T. (1998). Chlorophyll-specific
943 absorption coefficients and pigments of phytoplankton off Sanriku, northwestern north
944 Pacific. *Journal of Oceanography*, 54: 517–526. [https://doi.org/ 10.1007/BF02742453](https://doi.org/10.1007/BF02742453).

945 Tilstone, G.H., Miller, P.I., Brewin, R.J.W., & Priede, I. G. (2014). Enhancement of
946 primary production in the North Atlantic outside of the spring bloom, identified by
947 remote sensing of ocean colour and temperature. *Remote Sensing Environment*, 146, 77-
948 86. [https://doi.org/ 10.1016/j.rse.2013.04.021](https://doi.org/10.1016/j.rse.2013.04.021).

949 Triantafyllou, G., Yao, F., Petihakis, G., Tsiaras, K.P., Raitsos, D.E., Hoteit, I. (2014).
950 Exploring the Red Sea seasonal ecosystem functioning using a three-dimensional
951 biophysical model. *Journal of Geophysical Research*, 119 (3), 1791-1811. [https://doi.org/](https://doi.org/10.1002/2013JC009641)
952 [10.1002/2013JC009641](https://doi.org/10.1002/2013JC009641).

953 Uitz, J., Stramski, D., Reynolds, R.A., & Dubranna, J. (2015). Assessing phytoplankton
954 community composition from hyperspectral measurements of phytoplankton absorption

955 coefficient and remote-sensing reflectance in open-ocean environments. *Remote Sensing*
956 *Environment*, 171, 58-74. [https://doi.org/ 10.1016/j.rse.2015.09.027](https://doi.org/10.1016/j.rse.2015.09.027).

957 Uitz, J., Claustre, H., Gentili, B., & Stramski, D. (2010). Phytoplankton class-specific
958 primary production in the world's oceans: Seasonal and interannual variability from
959 satellite observations. *Global Biogeochemical Cycles*, 24, 1944-9224. [https://doi.org/](https://doi.org/10.1029/2009GB003680)
960 [10.1029/2009GB003680](https://doi.org/10.1029/2009GB003680).

961 Uitz, J., Huot, Y., Bruyant, F., Babin, M., & Claustre, H. (2008). Relating phytoplankton
962 photophysiological properties to community structure on large scales. *Limnology and*
963 *Oceanography*, 53 (2), 614-630. [https://doi.org/ 10.2307/40006445](https://doi.org/10.2307/40006445).

964 Uitz, J., Claustre, H., Morel, A., & Hooker, S. B. (2006). Vertical distribution of
965 phytoplankton communities in open ocean: An assessment based on surface chlorophyll.
966 *Journal of Geophysical Research*, 111 (C8), 2156-2202. [https://doi.org/](https://doi.org/10.1029/2005JC003207)
967 [10.1029/2005JC003207](https://doi.org/10.1029/2005JC003207).

968 Vault, D., & Partensky, E. (1992). Cell cycle of prochlorophytes in the north western
969 Mediterranean Sea. *Deep Sea Research*, 39 (5A), 727-742. [https://doi.org/ 10.1016/0198-](https://doi.org/10.1016/0198-0149(92)90117-C)
970 [0149\(92\)90117-C](https://doi.org/10.1016/0198-0149(92)90117-C).

971 Veldhuis, M.J.W., & Kraay, G. W. (1993). Cell abundance and fluorescence of
972 picoplankton in relation to growth irradiance and nitrogen availability in the Red Sea.
973 *Netherlands Journal of Sea Research*, 31 (2), 135-145. [https://doi.org/ 10.1016/0077-](https://doi.org/10.1016/0077-7579(93)90003-B)
974 [7579\(93\)90003-B](https://doi.org/10.1016/0077-7579(93)90003-B).

975 Vidussi, F., Claustre, H., Manca, B. B., Luchetta, A., & Marty, J. C. (2001).
976 Phytoplankton pigment distribution in relation to upper thermocline circulation in the
977 eastern Mediterranean Sea during winter. *Journal of Geophysical Research*, 106 (C9),
978 19939-19956. [https://doi.org/ 10.1029/1999JC000308](https://doi.org/10.1029/1999JC000308).

979 Vijayan, A.K., & Somayajula, S. A. (2014). Effect of accessory pigment composition on
980 the absorption characteristics of a dinoflagellate bloom in a coastal embayment.
981 *Oceanologia*, 56 (1), 107-124. <https://doi.org/0.5697/oc.56-1.107>.

982 Wafar, M., Ashraf, M., Manikandan, K. P., Qurban, M. A., & Kattan, Y. (2016).
983 Propagation of Gulf of Aden Intermediate Water (GAIW) in the Red Sea during autumn
984 and its importance to biological production. *Journal of Marine Systems*, 154, 243-251.
985 <https://doi.org/10.1016/j.jmarsys.2015.10.016>.

986 Wang, S.Q., Ishizaka, J., Hirawake, T., Watanabe, Y., Zhu, Y. L., Hayashi, M., & Yoo, S.
987 (2015). Remote estimation of phytoplankton size fractions using the spectral shape of
988 light absorption. *Optics Express*, 23 (8), 10301-10318. [https://doi.org/](https://doi.org/10.1364/OE.23.010301)
989 [10.1364/OE.23.010301](https://doi.org/10.1364/OE.23.010301).

990 Westberry, T.K., Dall'Olmo, G., Boss, E., Behrenfeld, M. J., & Moutin, T. (2010).
991 Coherence of particulate beam attenuation and backscattering coefficients in diverse open
992 ocean environments. *Optics Express*, 18 (15), 15419-15425. [https://doi.org/](https://doi.org/10.1364/OE.18.015419)
993 [10.1364/OE.18.015419](https://doi.org/10.1364/OE.18.015419).

994 Zinser, E.R., Johnson, Z. I., Coe, A., Karaca, E., Veneziano, D., & Chisholm, S. W.
995 (2007). Influence of light and temperature on *Prochlorococcus* ecotype distributions in the
996 Atlantic Ocean. *Limnology Oceanography*, 52 (5), 2205-2220. [https://doi.org/](https://doi.org/10.4319/lo.2007.52.5.2205)
997 [10.4319/lo.2007.52.5.2205](https://doi.org/10.4319/lo.2007.52.5.2205).

Figures legends

Figure 1: Map showing the locations of stations sampled during 5 cruises between October 2014 and January 2016 in the Red Sea (see Table 1). The delineation of the Northern Red Sea (NRS), the Central Red Sea (CRS) and the Southern Red Sea (SRS) is indicated on the map.

Map Produced using ArcGIS.

Figure 2: Variations of the particulate absorption coefficients at 440 nm, $a_p(440)$ (A), and at 676 nm, $a_p(676)$ (B), as a function of [TChl a]. The black and red solid lines represent the best fit (power law function) between $a_p(\lambda)$ and [TChl a] in all depth and within the first optical depth, respectively. The relationships from Bricaud et al. (1998) (dashed line) and Brewin et al. (2015) (dotted line) are displayed. Variations of the phytoplankton absorption coefficients at 440 nm, $a_{ph}(440)$ (C), and at 676 nm, $a_{ph}(676)$ (D), as a function of [TChl a]. The black and red solid lines represent the best fit (power law function) between $a_{ph}(\lambda)$ and [TChl a] in all depth and within the first optical depth, respectively. The relationships from Bricaud et al. (1995) (dashed-dotted line), Bricaud et al. (2004) (dashed line), Devred et al. (2006) (red dashed line) and Brewin et al. (2011) (blue dashed line) are displayed. The version of $a_{ph}(676)$ as a function of [TChl a] was not provided by Bricaud et al. (2004). The relationships of Devred et al. (2006), Brewin et al. (2011, 2015) are for 443 nm and 670 nm rather than 440 and 676 nm.

Figure 3: Variations of the absorption coefficient of non-algal particles at 440 nm, $a_{nap}(440)$, as a function of [TChl a] (A). The relationship provided by Bricaud et al. (2010) is displayed. Variations the non-algal to particulate absorption ratio, a_{nap}/a_p at 440 nm as a function of [TChl a].

Figure 4: Relative proportions (%) of microphytoplankton, nanophytoplankton and picophytoplankton estimated from the relative concentrations of some diagnostic pigments (equations (1)-(3)). For each sample the relative contribution of a size class to total biomass can be read on the corresponding axis as indicated.

Figure 5: Average of phytoplankton absorption spectra normalized by the average value of absorption between 400 and 700 nm shown separately for picophytoplankton-dominated samples (blue solid line), nanophytoplankton-dominated samples (red solid line) and microphytoplankton-dominated samples (green solid line). For each group of data, the mean normalized spectrum (solid line) and the standard deviation (dashed area) are displayed.

Figure 6: Variations of the cell size parameter (S_f) derived from the shape of the phytoplankton absorption spectrum as described by Ciotti et al. (2002) as a function of the proportions (%) of microphytoplankton (A) and picophytoplankton (B) estimated from the relative concentrations of some diagnostic pigments (equations (1)-(4)). The coefficient of determination was determined on the basis of all data in the form of a power law (A) and of a linear regression (B).

Figure 7: Variations of Chlorophyll specific phytoplankton absorption coefficients at 440 nm, $a_{ph(440)}^*$ (A), and at 676 nm, $a_{ph(676)}^*$ (B), as a function of [TChl *a*]. Samples are grouped for different ranges of cell size parameter (S_f) as indicated in the legend. The coefficient of determination was determined on the basis of all data in the form of a power law.

Figure 8: Variations of Chlorophyll specific phytoplankton absorption coefficients at 440 nm, $a_{ph(440)}^*$, as a function of the proportions (%) of microphytoplankton (A), nanophytoplankton (B), picophytoplankton (C) estimated from the relative concentrations of some diagnostic pigments (equations (1)-(3)) and the cell size parameter (S_f) (D) derived from the shape of the phytoplankton absorption spectrum as described by Ciotti et al. [2002]. Samples are grouped for different ranges of cell size parameter (S_f) as indicated in the legend.

The coefficient of determination was determined on the basis of all data in the form of a power law (A, B) and of a linear regression (C, D).

Figure 9: Variations of Chlorophyll specific phytoplankton absorption coefficients at 440 nm, $a_{ph(440)^*}$, as a function of the accessory pigments to [TChl *a*] ratios: the ratio of total chlorophyll b [TChl b] to [TChl *a*] (A); the ratio of total chlorophyll c [TChl c] to [TChl *a*] (B); the ratio of photosynthetic carotenoids PSC to [TChl *a*] (C) and the ratio of photoprotective carotenoids PPC to [TChl *a*] (D). Samples are grouped for different ranges of cell size parameter (S_f) as indicated in the legend. The coefficient of determination was determined on the basis of all data in the form of a power law (B, C) and of a linear regression (C, D).

Figure 10: Variations of the size index (SI) estimated from the relative concentrations of some diagnostic pigments (equations (1)-(5)) (A) as a function of [TChl *a*] and average (filled circle) \pm standard deviation (empty circle) SI values (B); variations of the PPC/ [TChl *a*] ratios as a function of [TChl *a*] (C) and average (filled circle) \pm standard deviation (empty circle) PPC/ [TChl *a*] values (F) for various areas of the global ocean. Data collected during cruises other than those performed in the Red Sea are taken from Bricaud et al. (2004, 2010).

Figure 11: Latitudinal variations of Chlorophyll specific phytoplankton absorption coefficients at 440 nm, $a_{ph(440)^*}$ (A), Temperature (B) and salinity (C). The delineation of the Northern Red Sea (NRS), the Central Red Sea (CRS) and the Southern Red Sea (SRS) is indicated on each panel. Samples are grouped according to the phytoplankton dominated group (mico-, nano- or picophytoplankton) as indicated in the legend.

Figure 1

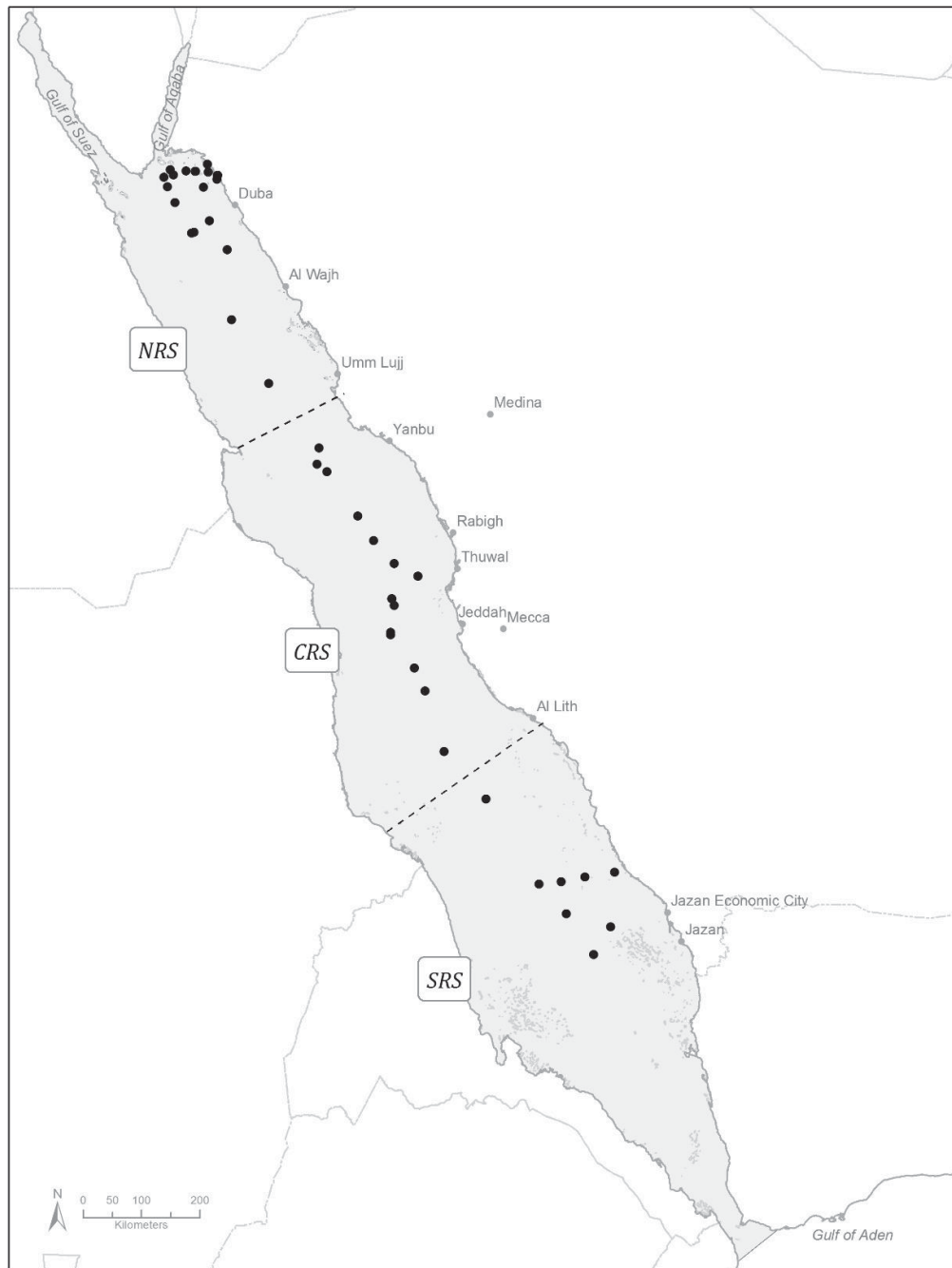


Figure 2

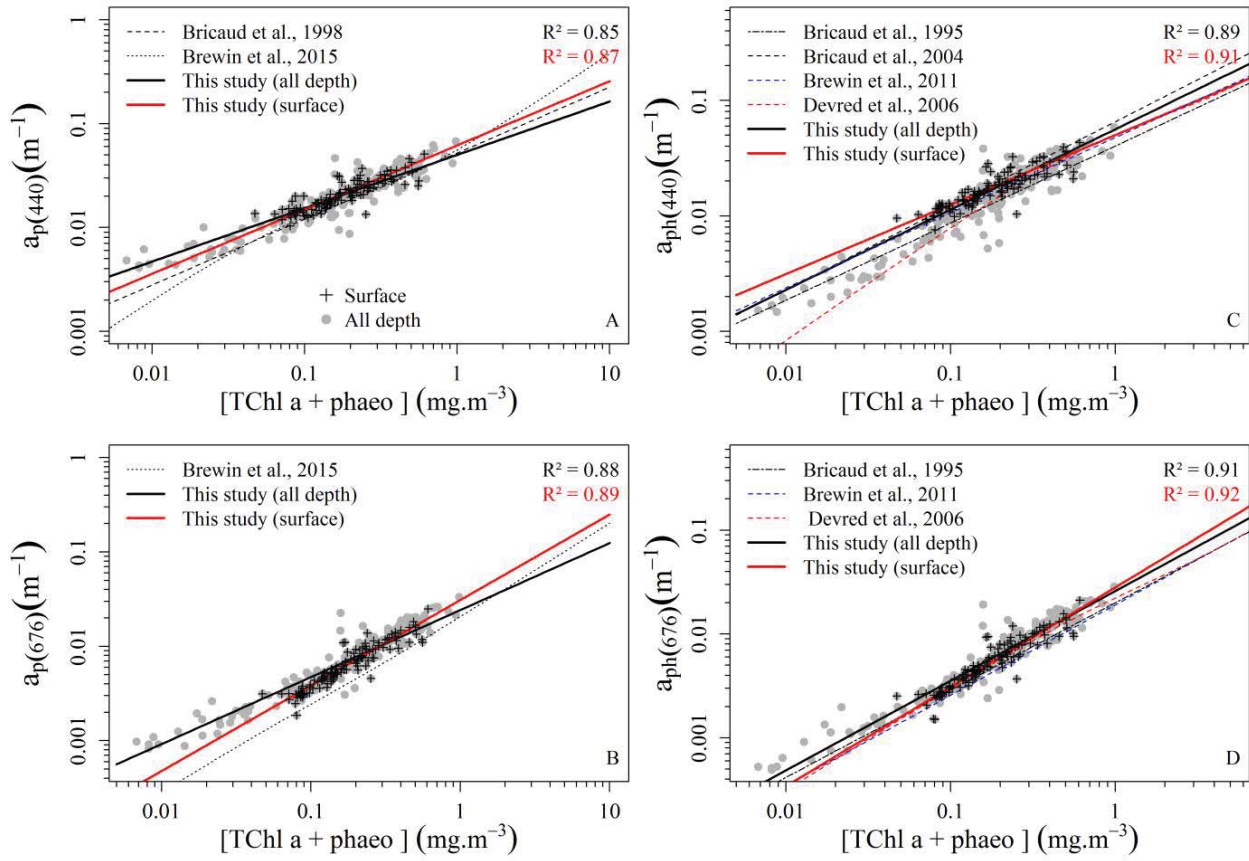


Figure 3

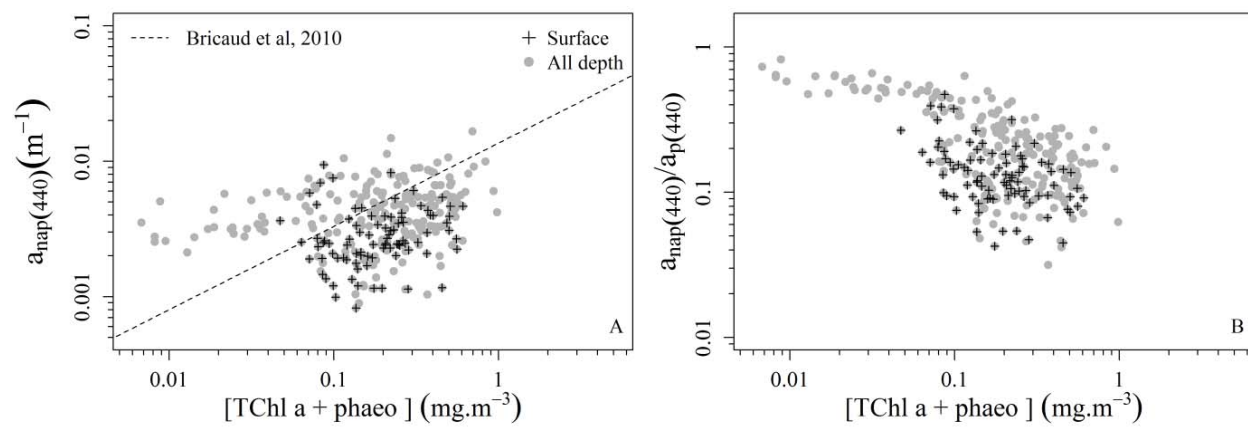


Figure 4

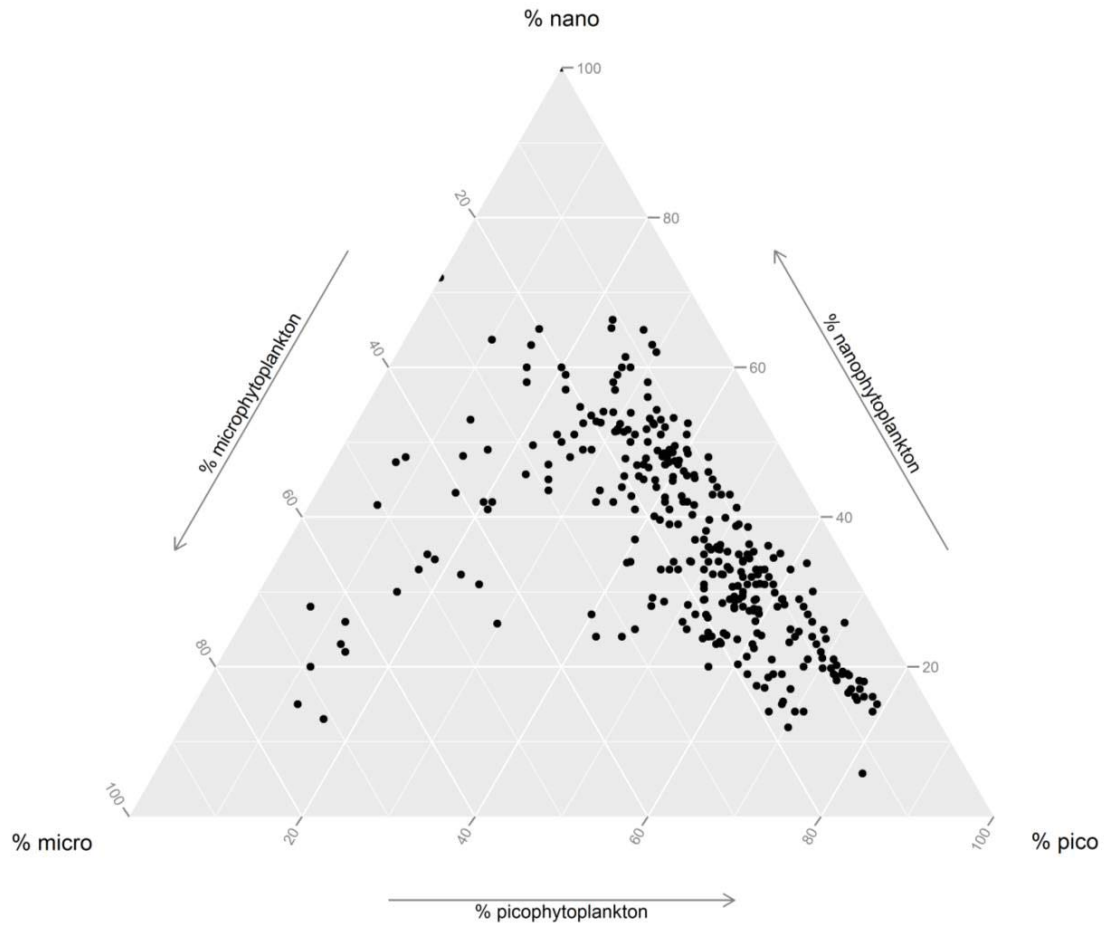


Figure 5

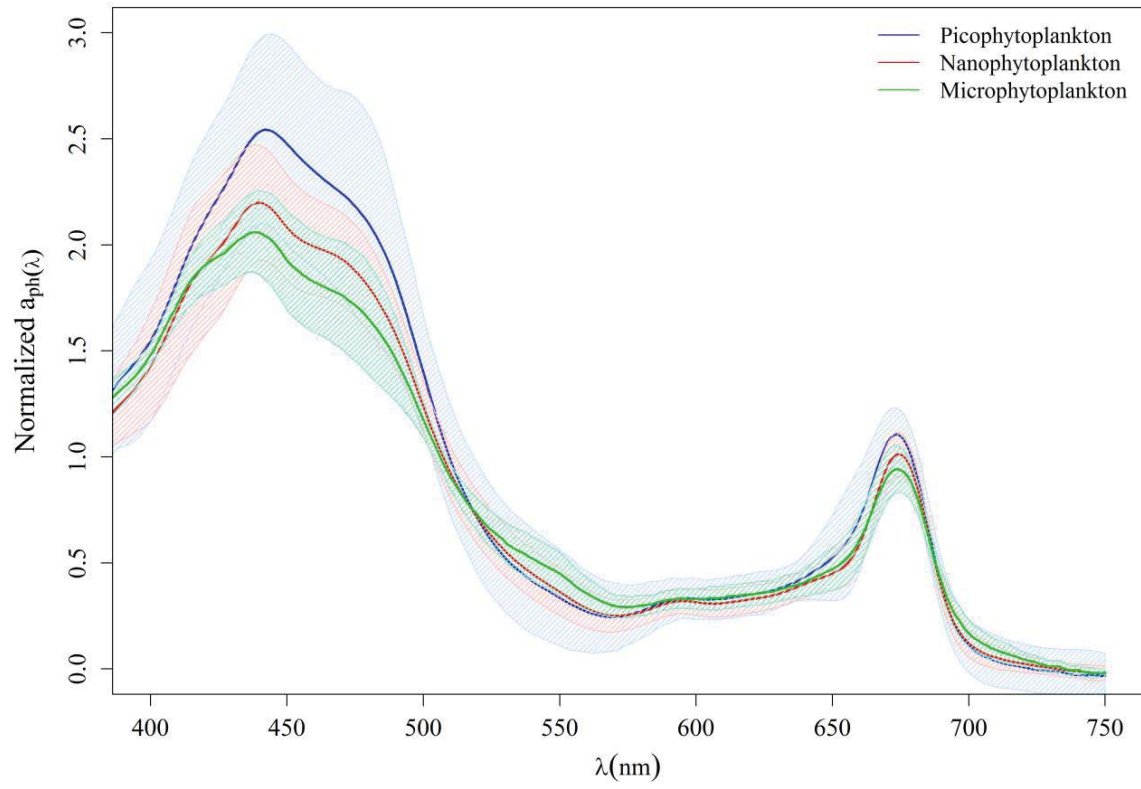


Figure 6

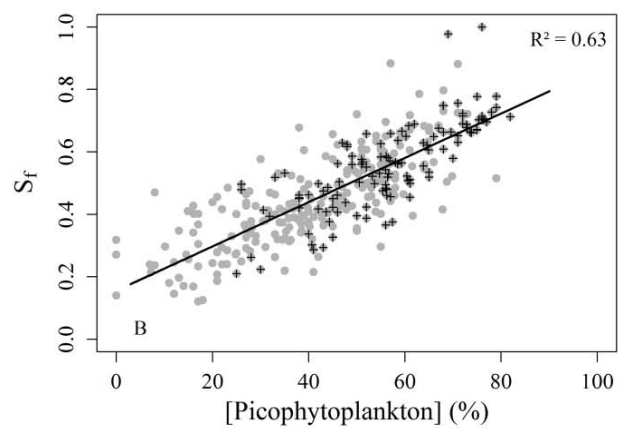
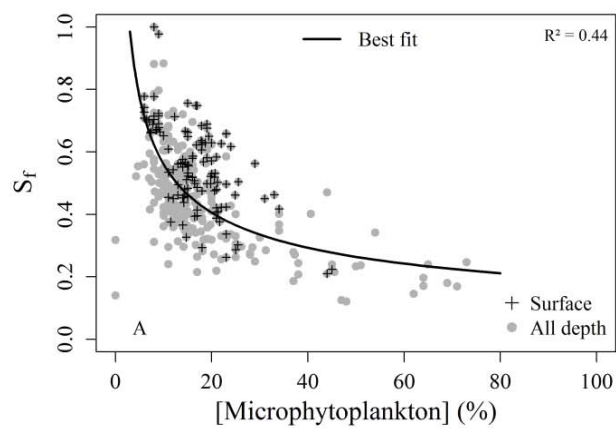


Figure 7

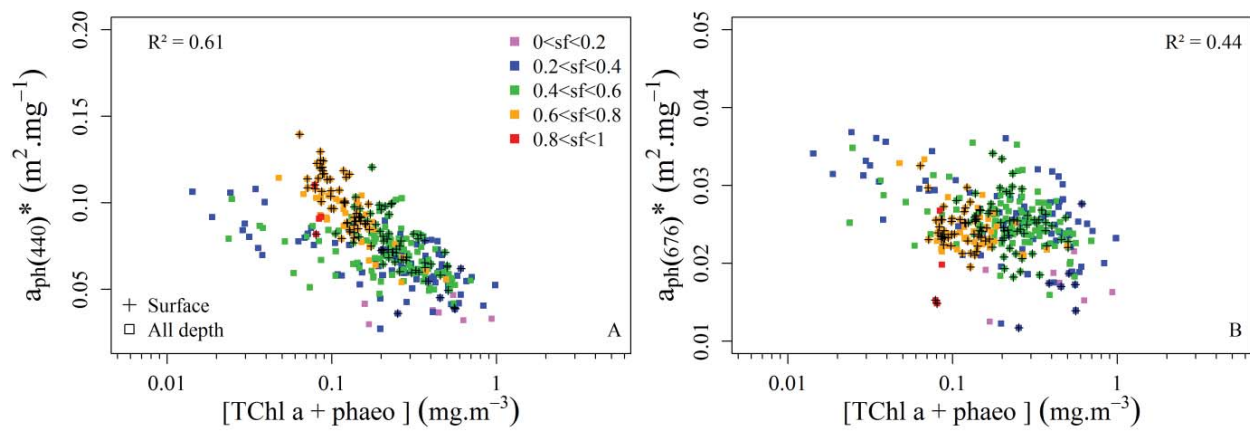


Figure 8

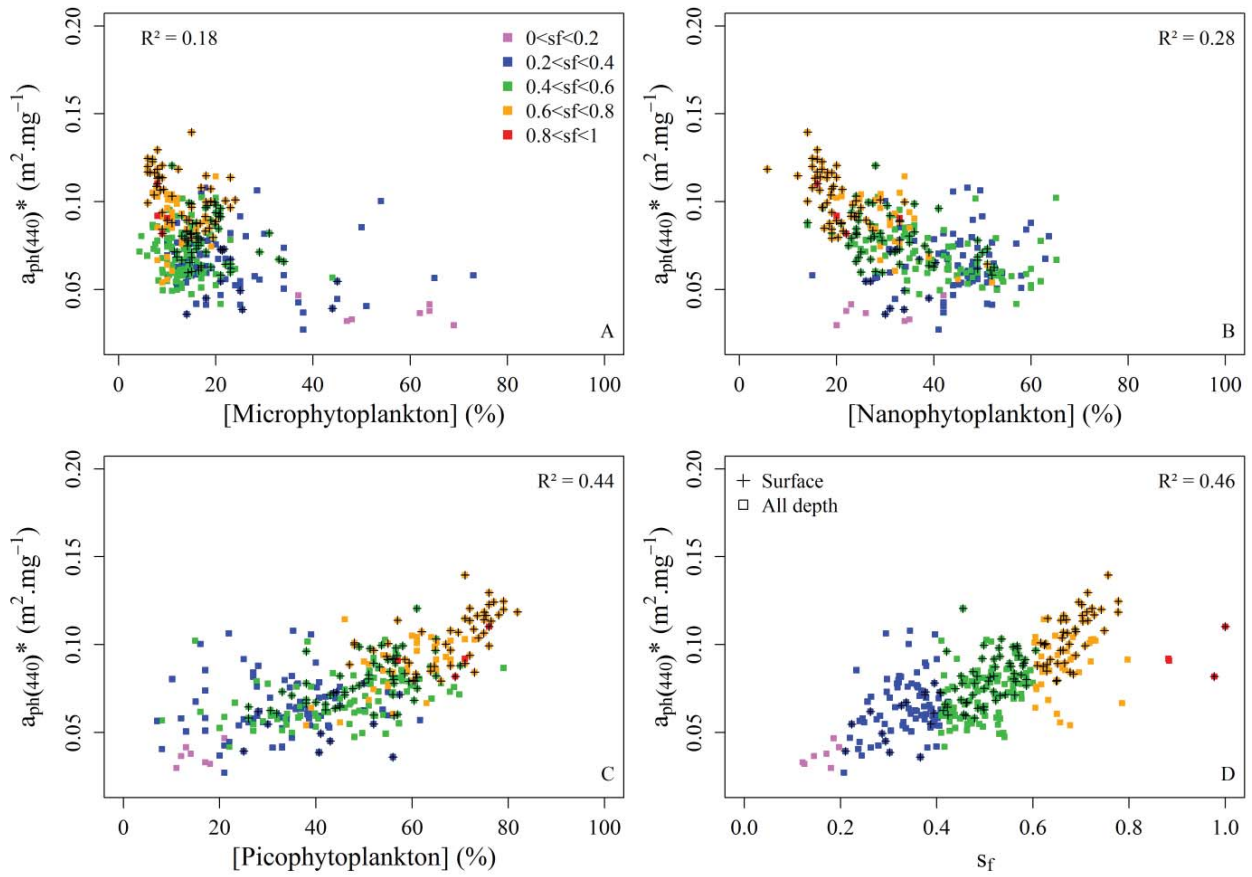


Figure 9

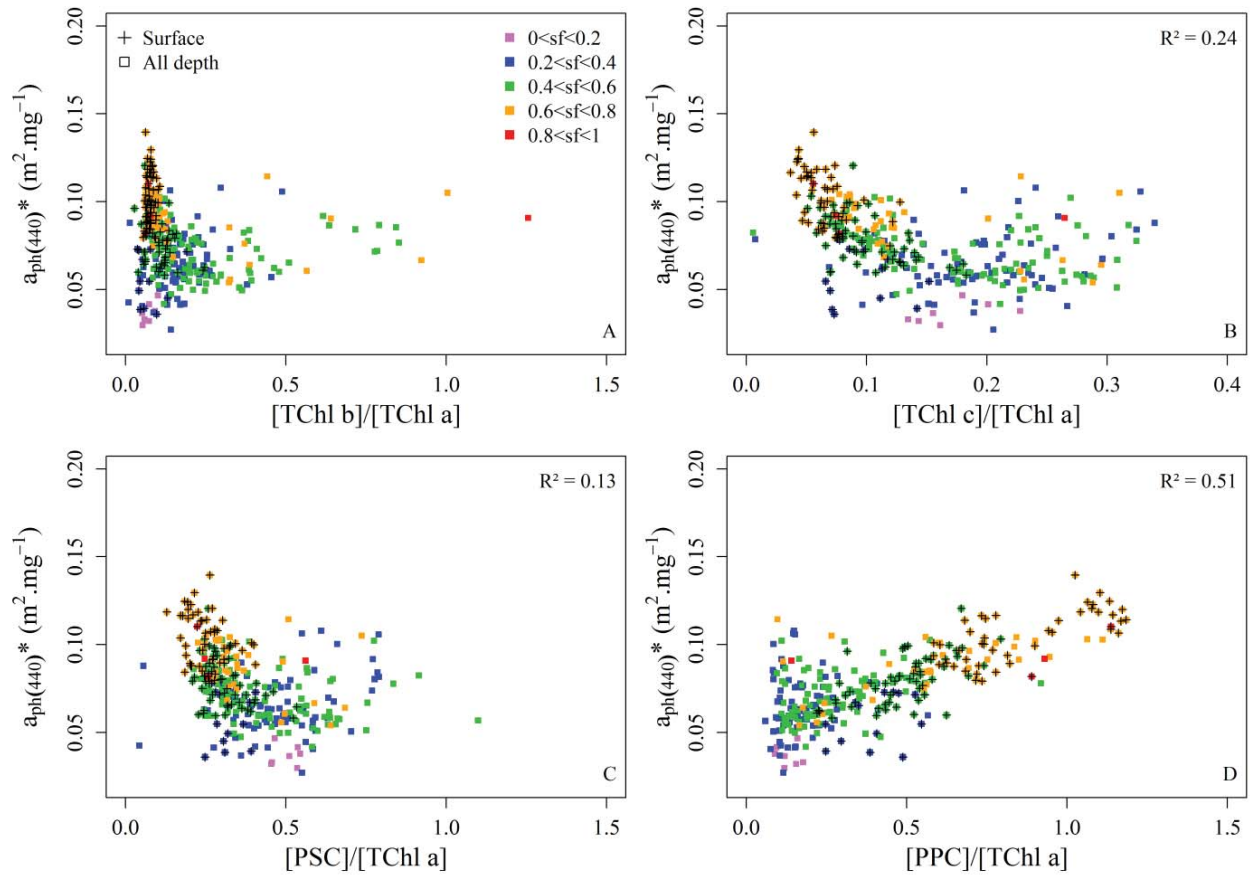


Figure 10

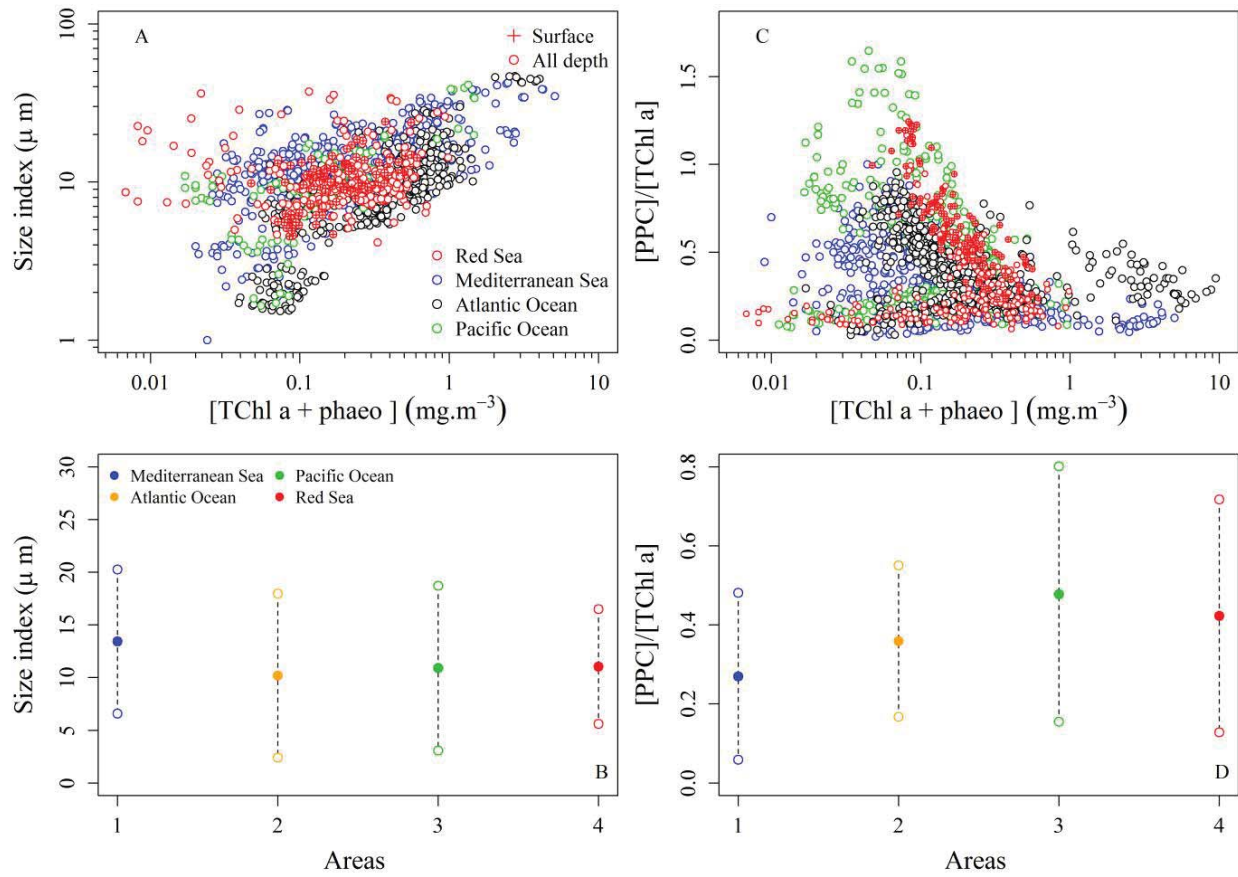
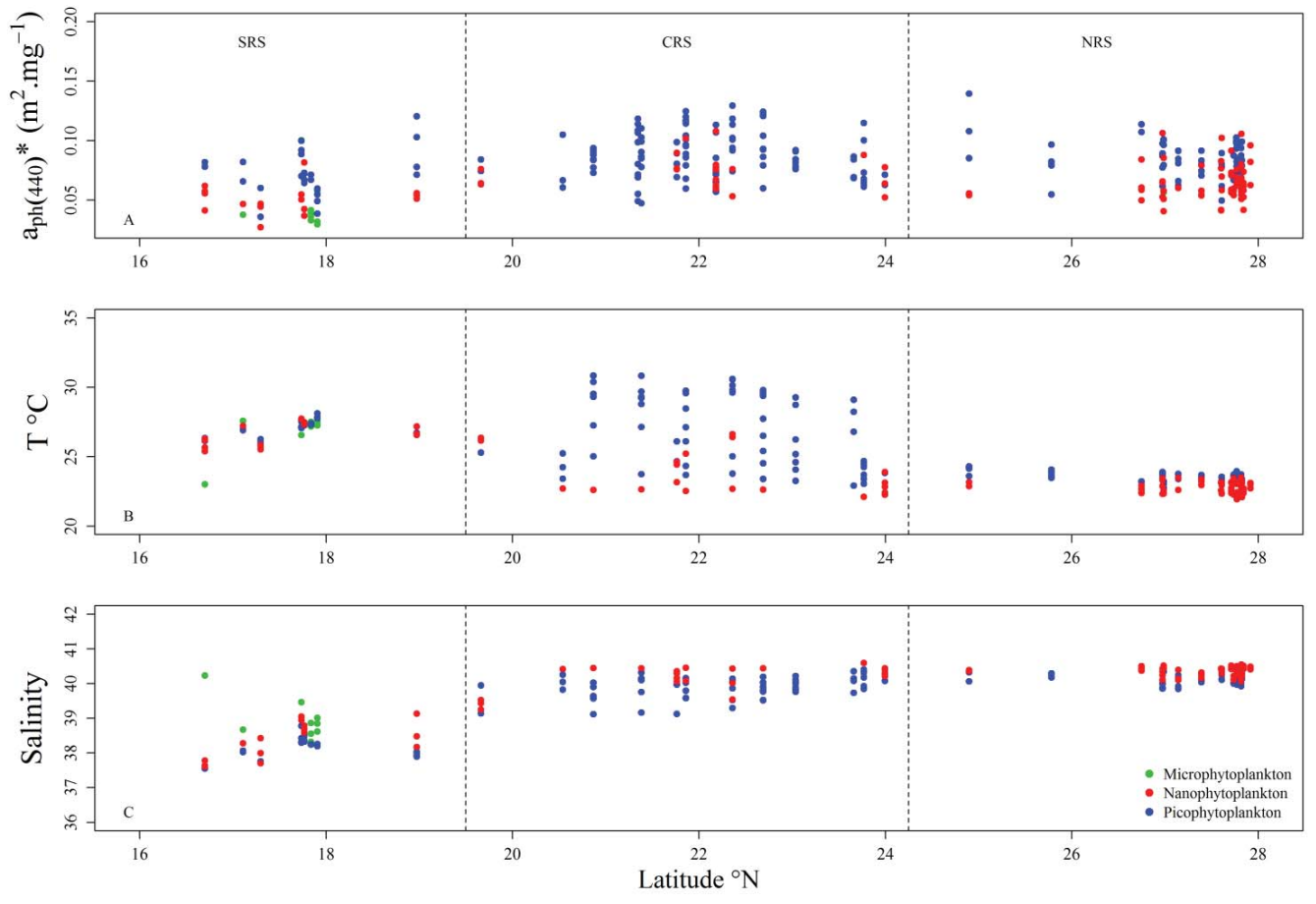


Figure 11



Tables

Table 1: Location and dates of the 5 sampling cruises in the Red Sea.

Campaign	Platform	Location	Abbreviation	Period	Number of stations
Nutrient cycle cruise 1	RV <i>Thuwal</i>	Central Red Sea	CRS-01	16-28 Oct. 2014	8
Jazan cruise	RV <i>Thuwal</i>	Southern Red Sea	Jazan	8 -21 Feb. 2015	8
Duba cruise 1	RV <i>Thuwal</i>	Northern Red Sea	Duba-01	17- 28 Apr. 2015	10
Duba cruise 2	RV <i>Thuwal</i>	Northern Red Sea	Duba-02	21 Mar. to 02 Apr. 2016	8
Nutrient cycle cruise 4	RV <i>Thuwal</i>	Central Red Sea	CRS-04	17-28 Jan. 2016	6
Total					40

Table 2: Results from the regression^a analysis between $a_p(440)$, $a_p(676)$, $a_{ph}(440)$, $a_{ph}(676)$ and [TChl *a*] among all depths and within the surface layer presented in Figure 2

		$a_p(440)$	$a_p(676)$	$a_{ph}(440)$	$a_{ph}(676)$
All depths	A	0.05	0.024	0.056	0.026
	B	0.51	0.71	0.70	0.87
	R ²	0.85	0.88	0.89	0.91
	N			297	
Surface	A	0.062	0.031	0.050	0.028
	B	0.62	0.90	0.60	0.96
	R ²	0.87	0.89	0.91	0.92
	N			108	

^a The regression formula is in the form of a power law as $X = A [TChl a]^B$ where A and B are the best fit parameters. The determination coefficient, R², and the number of data, N, are also shown. All regressions are significant for $p < 0.0001$.

Figure 1.

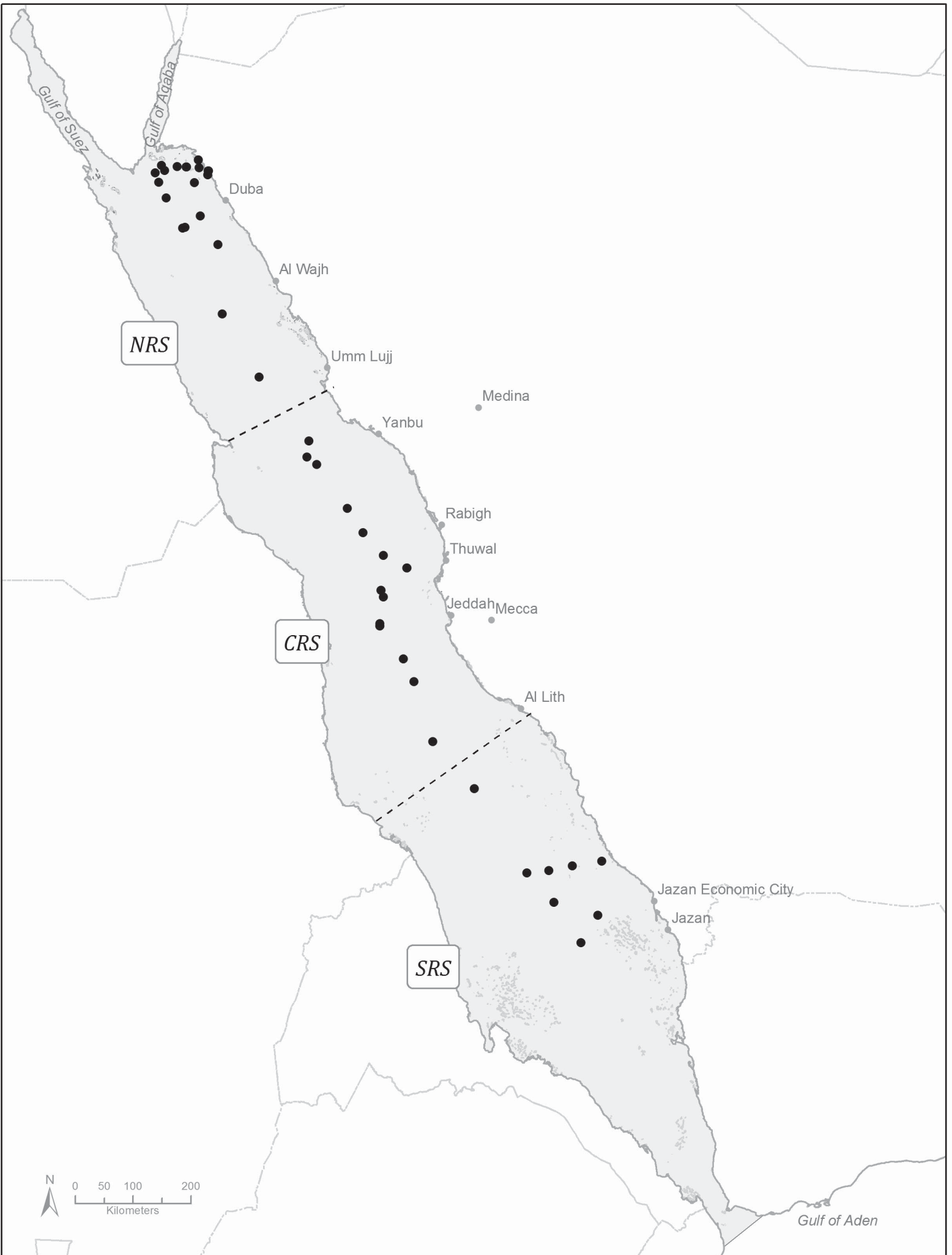


Figure 2.

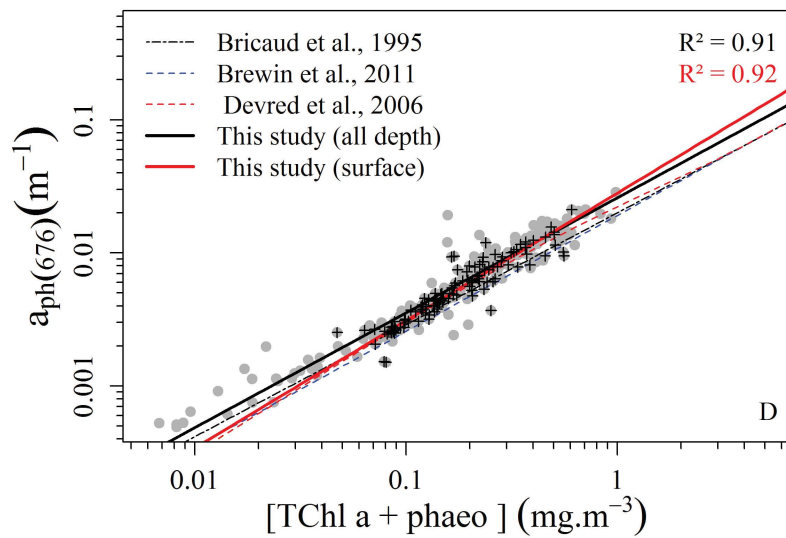
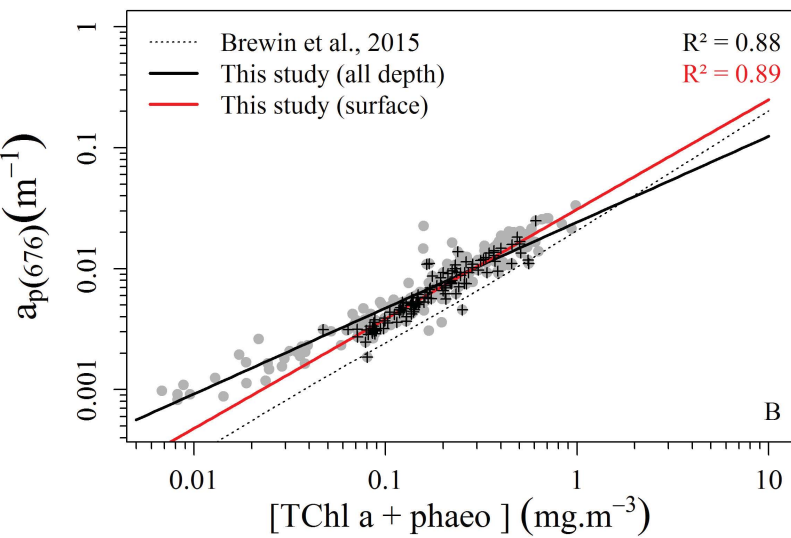
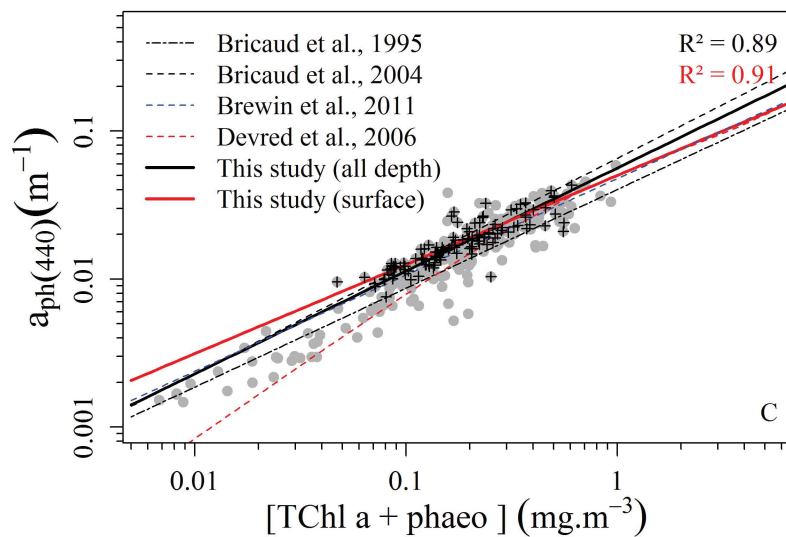
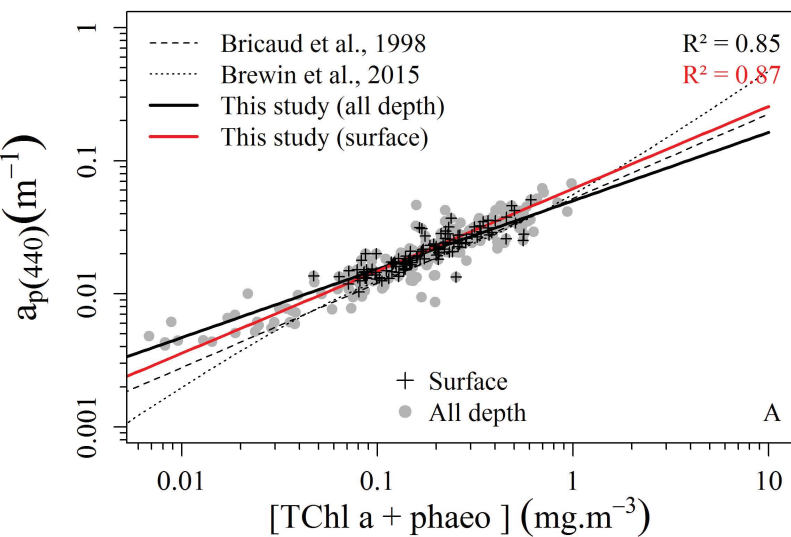


Figure 3.

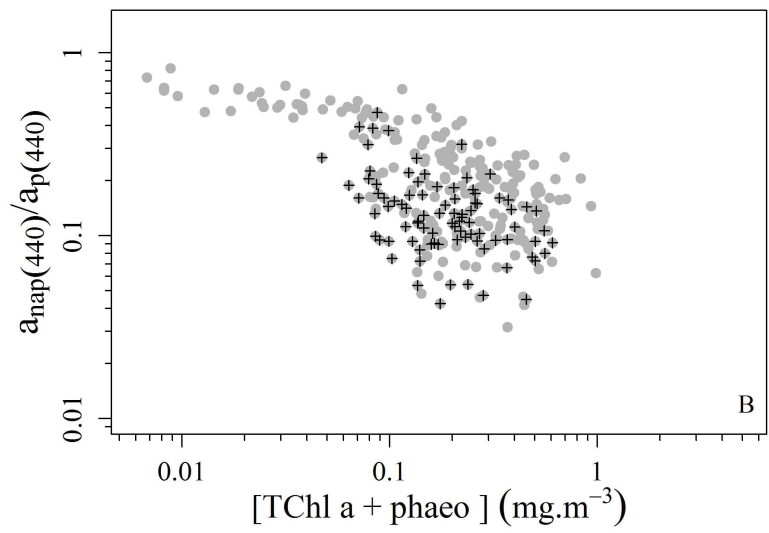
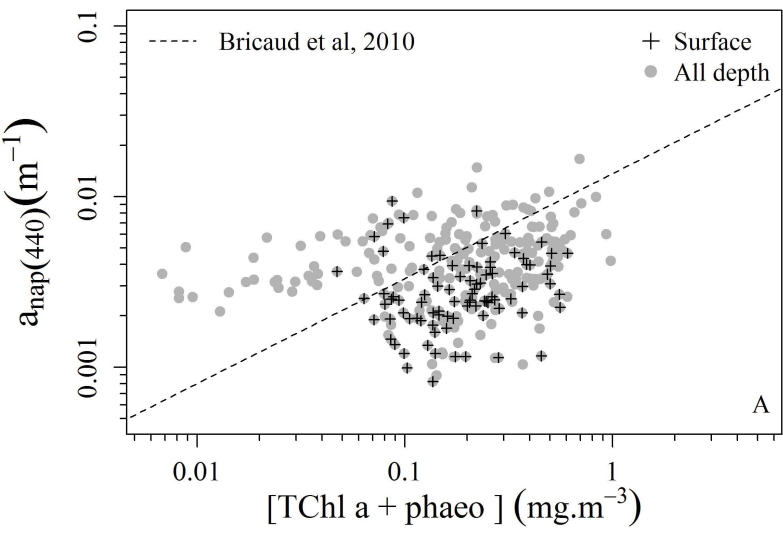


Figure 4.

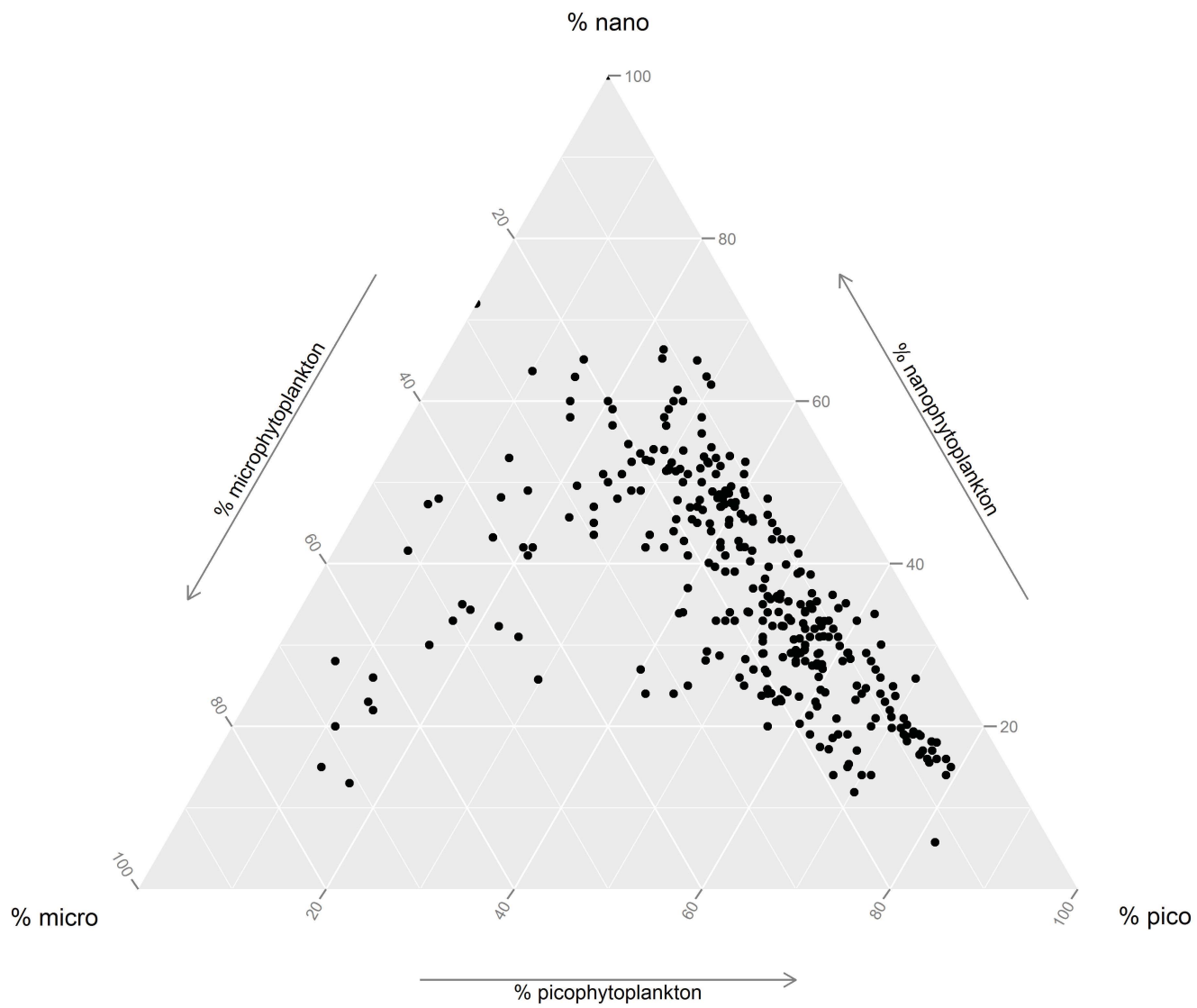


Figure 5.

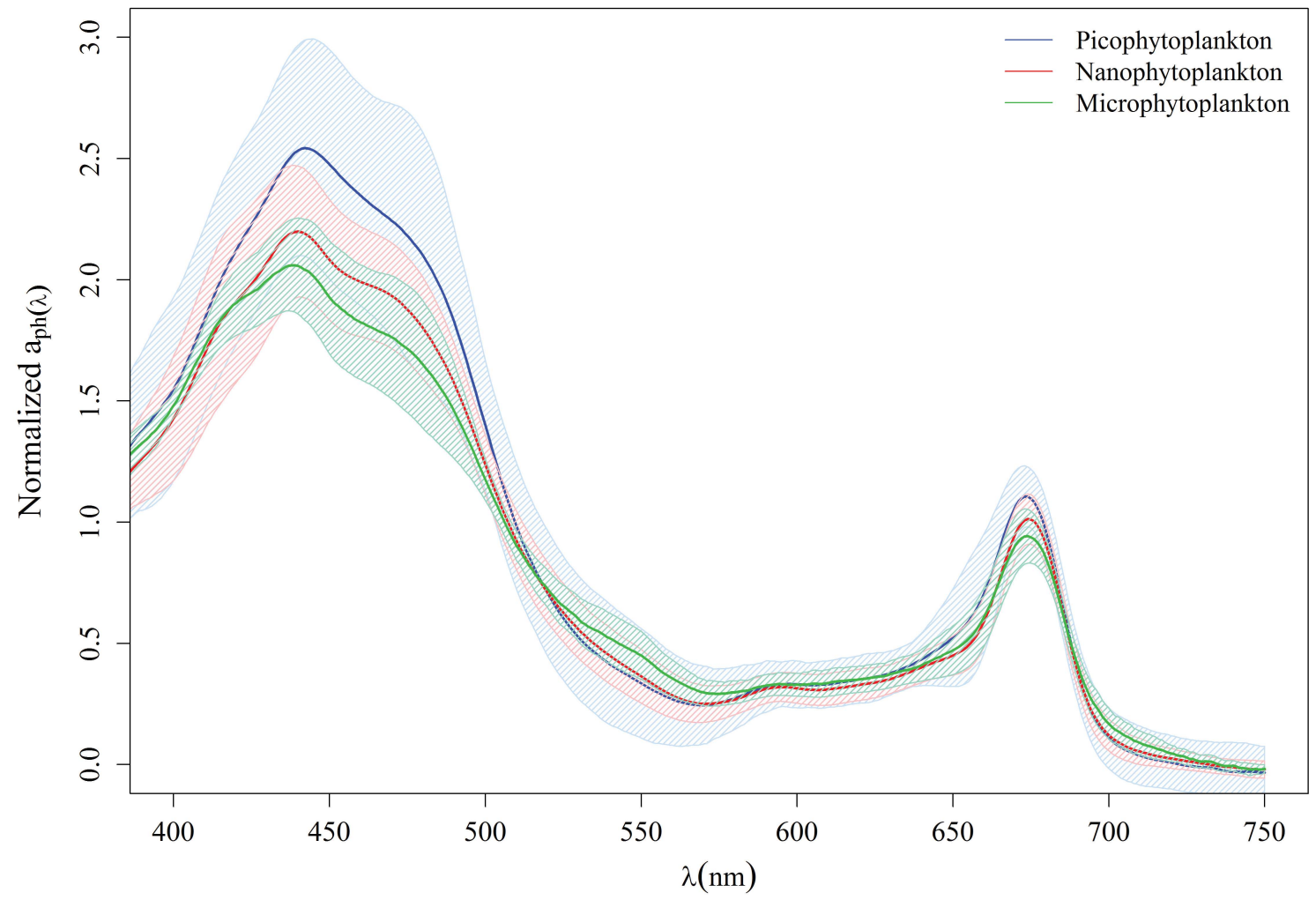


Figure 6.

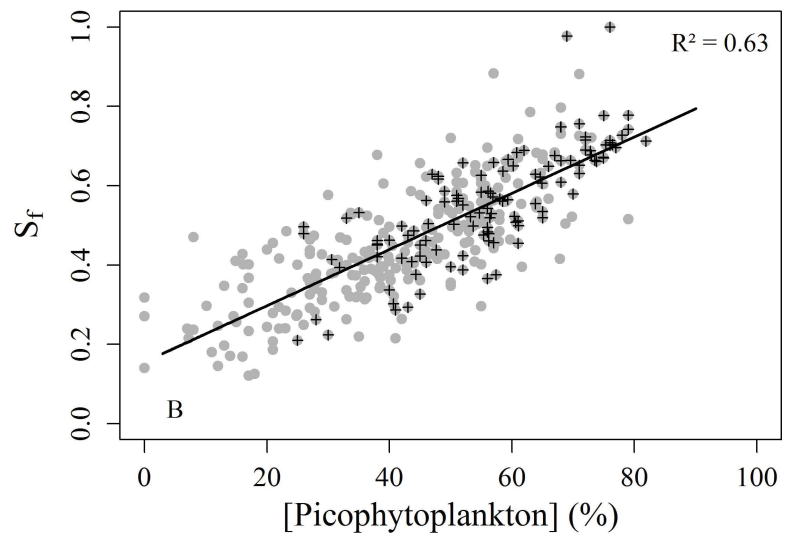
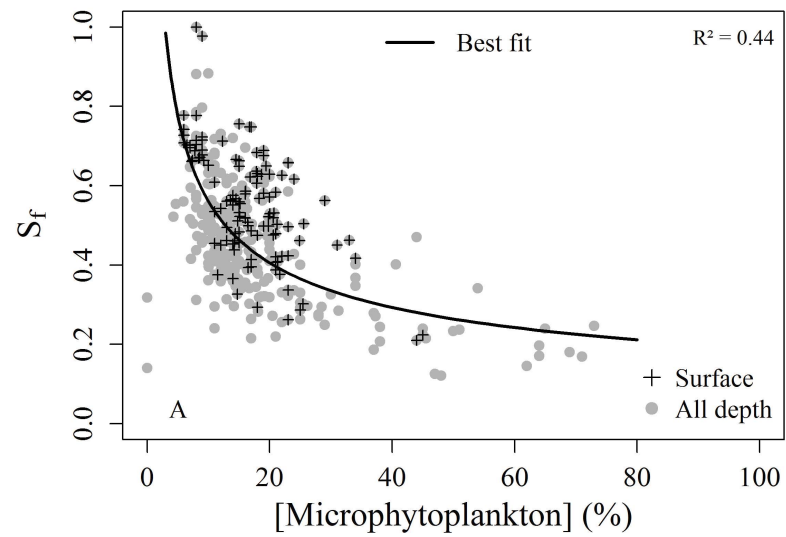


Figure 7.

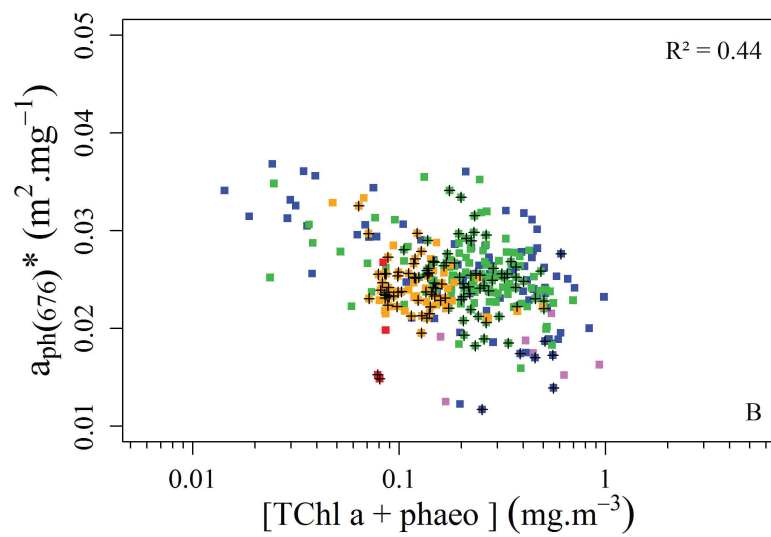
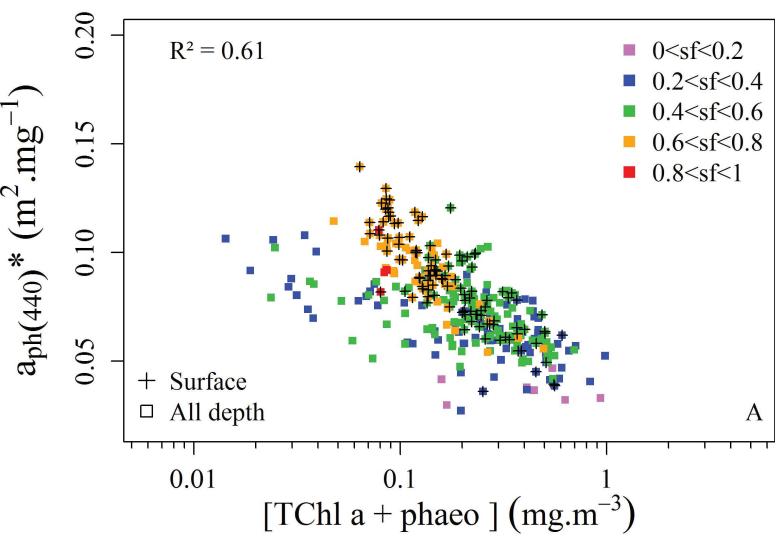


Figure 8.

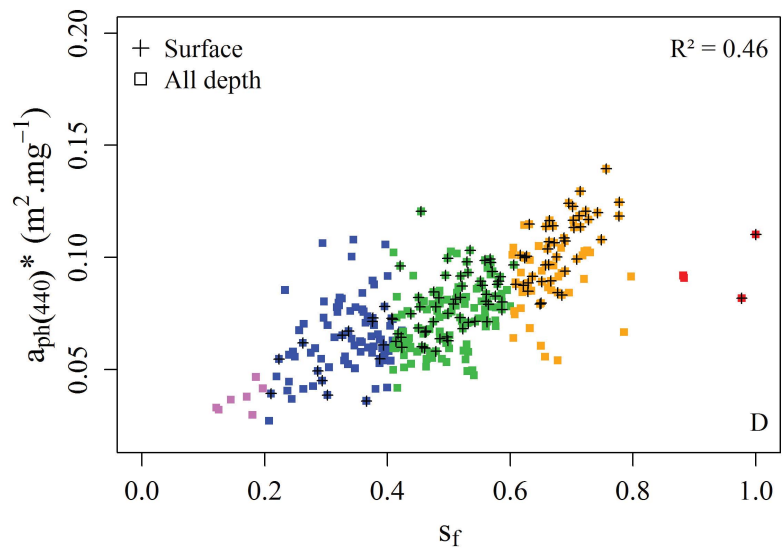
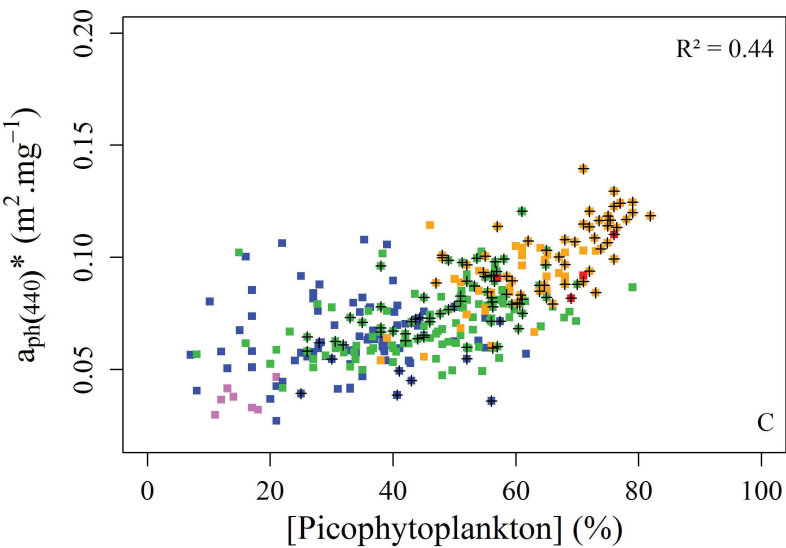
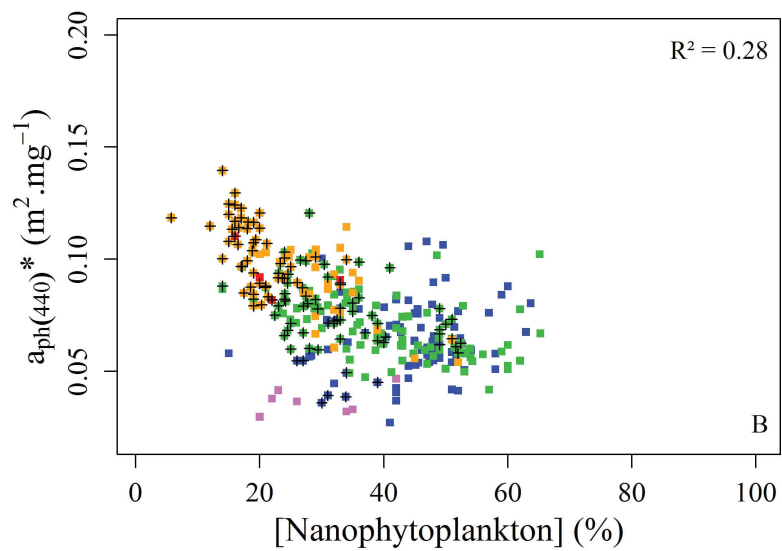
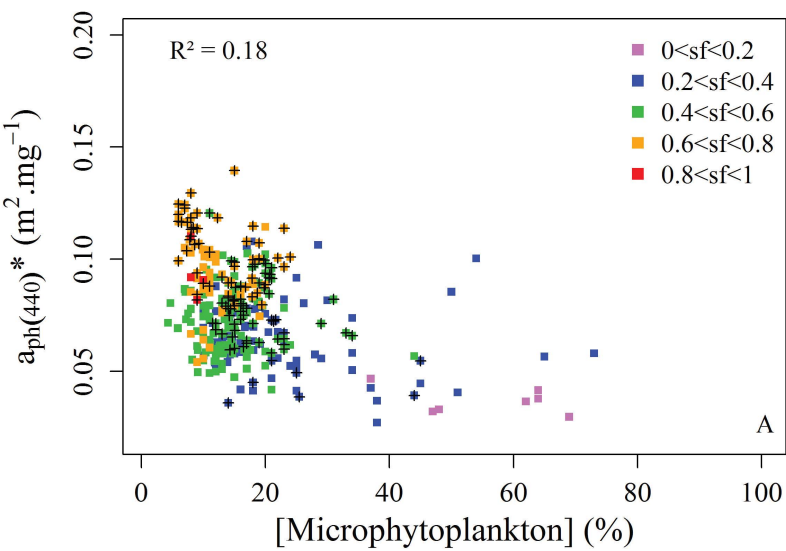


figure 9.

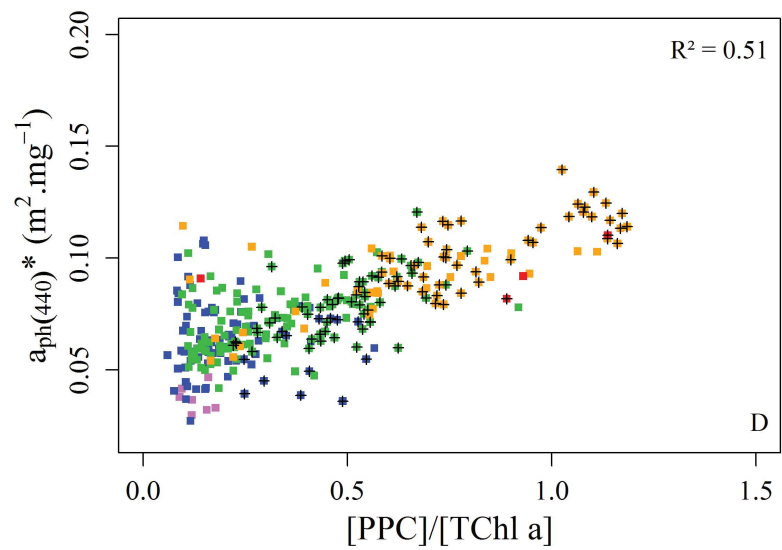
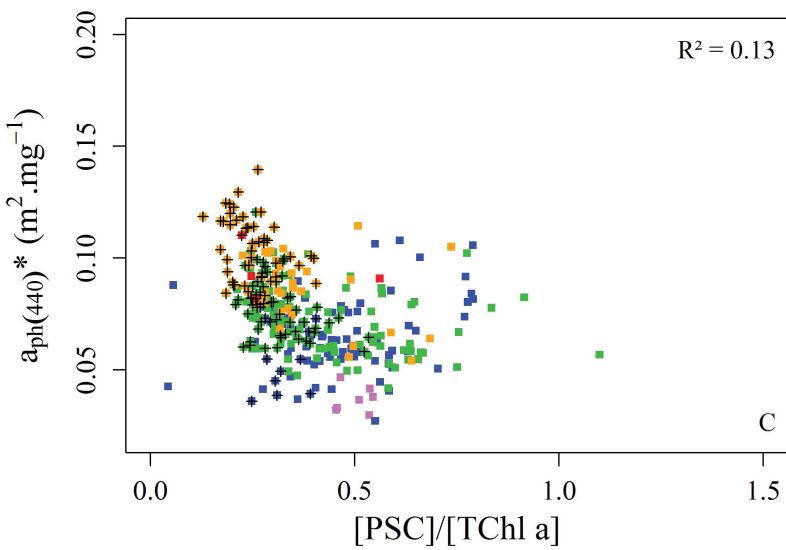
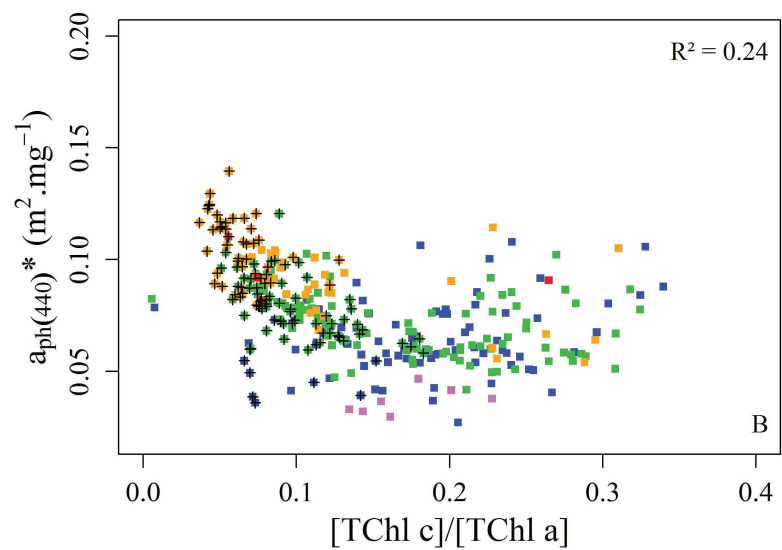
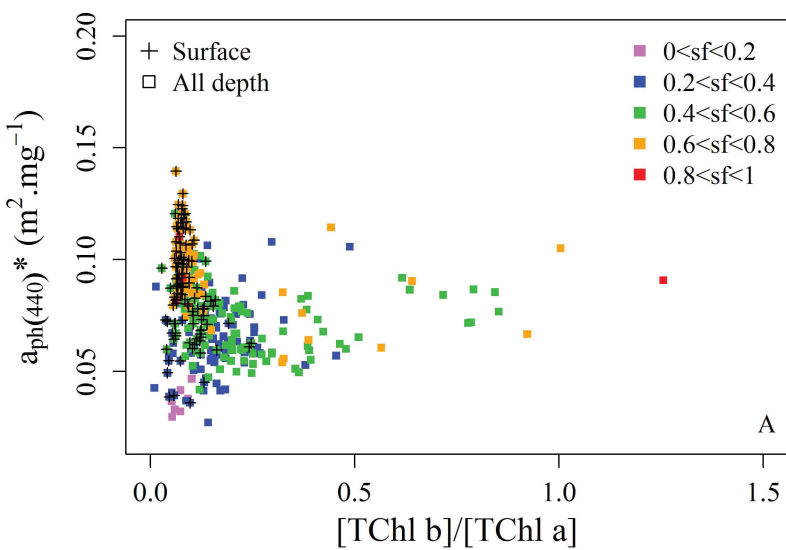


Figure 10.

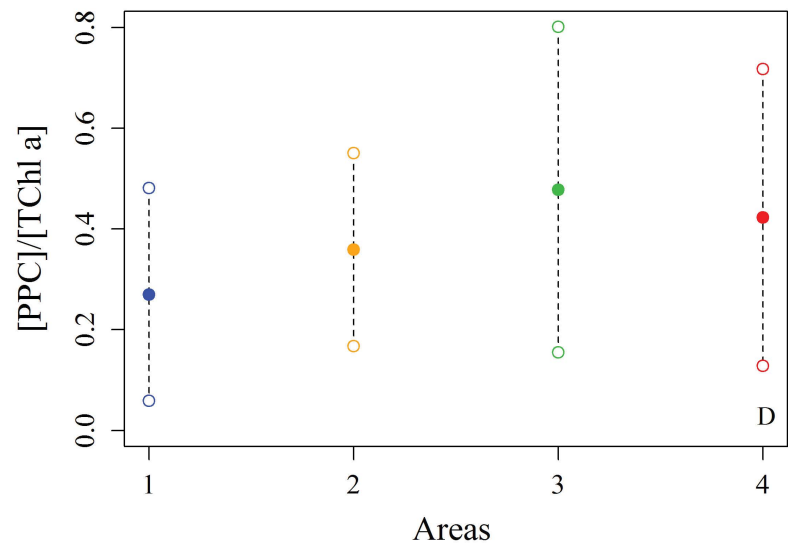
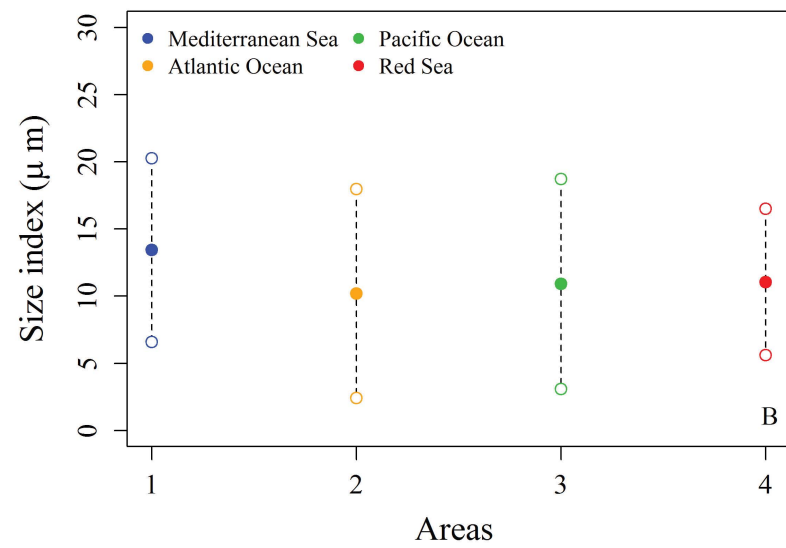
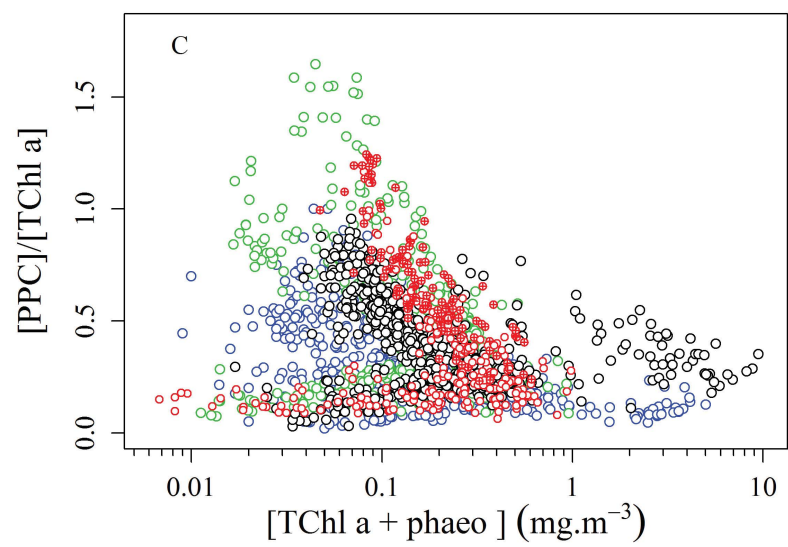
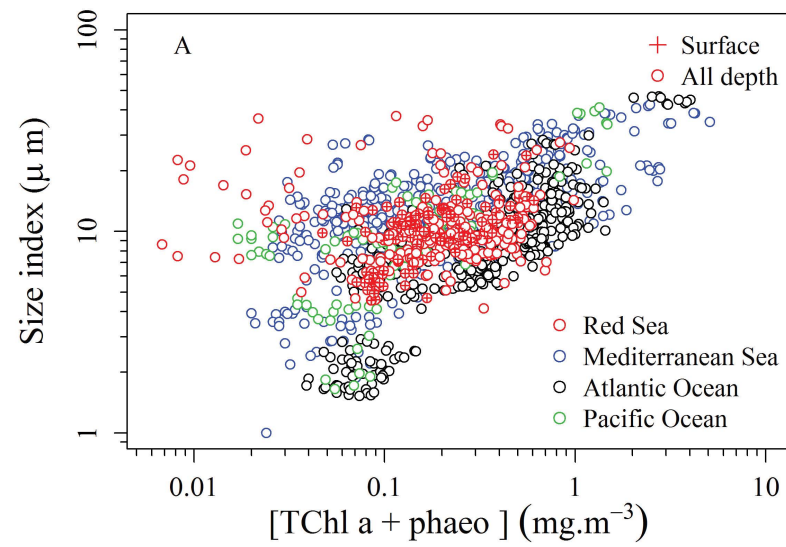


Figure 11.

